Brigham Young University

BYU ScholarsArchive

2009-03-12

Developing Response Surfaces Based on Tool Geometry for a Convex Scrolled Shoulder Step Spiral (CS4) Friction Stir Processing Tool Used to Weld AL 7075

Bryce K. Nielsen
Brigham Young University - Provo

Follow this and additional works at: https://scholarsarchive.byu.edu/etd

Part of the Mechanical Engineering Commons

DEVELOPING RESPONSE SURFACES BASED ON TOOL GEOMETRY FOR A

CONVEX SCROLLED SHOULDER STEP SPIRAL (CS4) FRICTION STIR

PROCESSING TOOL USED TO WELD AL 7075

by

Bryce Nielsen

A thesis submitted to the faculty of

Brigham Young University

in partial fulfillment of the requirements for the degree of

Master of Science

Department of Mechanical Engineering

Brigham Young University

April 2009

BRIGHAM YOUNG UNIVERSITY

GRADUATE COMMITTEE APPROVAL

of a thesis submitted by

Bryce Nielsen

This thesis has been read by each member of the following graduate committee and by majority vote has been found to be satisfactory.

_____	_____
Date	Carl D. Sorensen, Chair
_____	_____
Date	Tracy W. Nelson
_____	_____
Date	Michael P. Miles

BRIGHAM YOUNG UNIVERSITY

As chair of the candidate's graduate committee, I have read the thesis of Bryce Nielsen in its final form and have found that (1) its format, citations, and bibliographical style are consistent and acceptable and fulfill university and department style requirements; (2) its illustrative materials including figures, tables, and charts are in place; and (3) the final manuscript is satisfactory to the graduate committee and is ready for submission to the university library.

_____
Date

_____
Carl D. Sorensen
Chair, Graduate Committee

Accepted for the Department

_____
Larry L. Howell
Graduate Coordinator

Accepted for the College

_____
Alan R. Parkinson
Dean, Ira A. Fulton College of Engineering and Technology

ABSTRACT

DEVELOPING RESPONSE SURFACES BASED ON TOOL GEOMETRY FOR A

CONVEX SCROLLED SHOULDER STEP SPIRAL (CS4) FRICTION STIR

PROCESSING TOOL USED TO WELD AL 7075

Bryce Nielsen

Department of Mechanical Engineering

Master of Science

The purpose of this study is to develop a series of response surfaces that define

critical outcomes for welding in Al 7075 based on the tool geometry of a convex scrolled

shoulder step spiral (CS4) friction stir processing tool. These response surfaces will be

used to find critical minimums in forces which will decrease the required power input for

the process. A comprehensive parameterization of the tool geometry is defined in this

paper. A pilot study was performed to determine the feasibility of varying certain

geometric features. Then a screening experiment eliminated those geometric features that

were not as significant in determining the response surfaces. A central composite design

with the five most important geometric features was used in order to develop response

surfaces for nine different response variables. The nine response variables are the

longitudinal, lateral and axial forces; the tool temperature, the spindle torque, the amount

of flash, the presence of defects, the surface roughness and the ledge size. By using standard regression techniques, response surface equations were developed that will allow the user to optimize tool geometries based on the desired response variables. The five geometric features, the process parameters and several of their interactions were found to be highly significant in the response surfaces.

ACKNOWLEDGMENTS

TABLE OF CONTENTS

LIST OF TABLES

xi

LIST OF FIGURES

1   Introduction

Friction Stir Welding (FSW) is a relatively new process that has been found to significantly improve on traditional arc welding techniques. The process involves a rotating cylindrical tool with a smaller projecting probe that plunges into the seam of the material to be welded. The friction from the rotating contact surface heats and softens the workpiece and then mixes the material from the two plates together as shown in Figure 1-1.
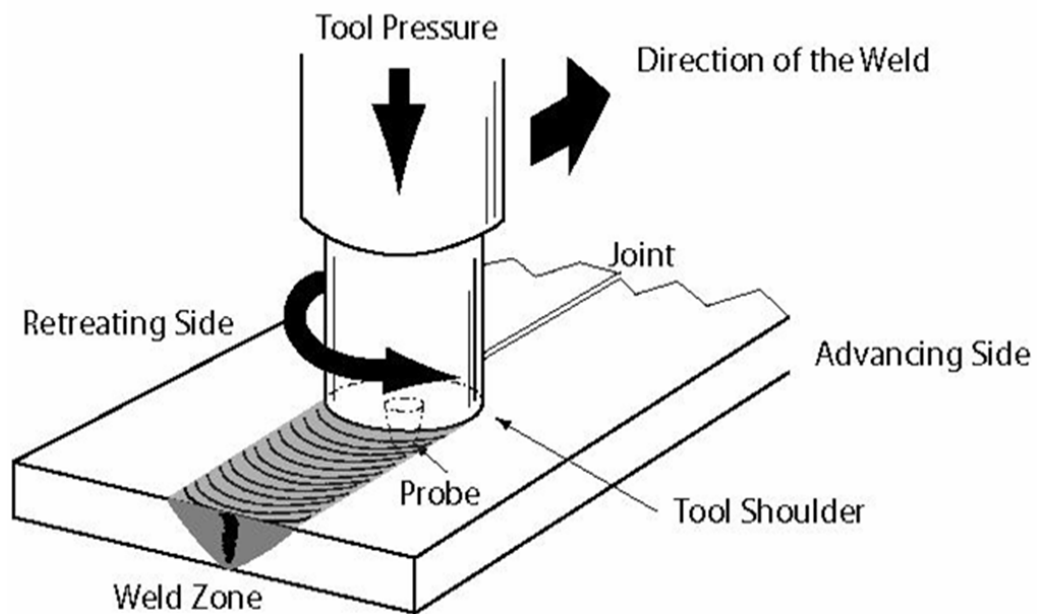
Figure 1-1: Friction Stir Process [1]

1

The advantages to this type of welding, compared to more traditional types of welding, consist mainly in better post-weld material properties. The temperatures involved with FSW are lower in most cases, which produces a smaller heat-affected zone (HAZ). With the lower temperatures, the workpiece material does not reach the melting point, which is a great advantage especially for welding aluminum. Additionally, the toughness and strength of the welds are generally higher than fusion welds. During the stirring process, plastic strain produces interesting microstructures that oftentimes have favorable material properties. The process is also less toxic than arc welding.

One of the disadvantages of this process is the cost of equipment. The process requires significant process forces and much larger machinery than other types of welding. FSW is also less capable of handling complex geometries because of these increased process forces. Changing the geometry of the tool will potentially decrease these process forces and thereby reduce the cost and improve the capability of FSW.

Most of the experimentation with the geometry of FSW tools has been "trial and error", with the observation that some tools seem to work better in certain situations than other tools. It can only be assumed that private organizations have done more extensive studies of FSW tool geometry in order to maximize the capabilities of their tools, but they are obviously less willing to share their results with competitors. This study closely examines the CS4 tool in order to find out which of the geometric features are responsible for this improved performance and determine the optimum geometry for the tools to run with maximum efficiency.

There are several ways to judge the value of a weld. There may be different optimum outcomes based on the minimum quality of weld desired and the limitations of

the equipment available to run the weld. For example, someone may want a weld with a minimum tensile strength that can be achieved while minimizing the cost of production. Another application may require the weld with the smoothest surface finish or the best strength, without regard to cost. Therefore the objective of this research is to map out a response surface that will predict the process forces, the tool temperature, and the surface quality of the weld based on the tool geometry and the process parameters.

Because of the large quantity of tools that were anticipated for this study, it was decided that the experimentation would be done with aluminum as the workpiece. Al 7075 T-651 was chosen and 9.5 mm (.375 in) thick plates were used as the processed material throughout this study. It is hoped that the results of this study will give insight into optimal tool geometries for other weld materials even though the response surfaces may not be exactly the same.

This thesis describes the previous work that has been done with different tool designs and then addresses the phases of the research process that were followed for this study. First, the tool geometry was defined and particular parameters were identified for inclusion in this study. Second, a pilot study was conducted to determine the feasibility and effectiveness of varying some of the key geometric features. Third, a screening experiment eliminated the variables that are not significant. Finally, a central composite design was used to determine the response surface.

2 Previous Work

As the friction stir process has evolved, there have been several styles of tool geometry that have been tried. Some of the existing geometries for the shoulder include: a smooth, concave surface; a scrolled, flat surface; a scrolled, tapered surface and others as shown in Figure 2-1.
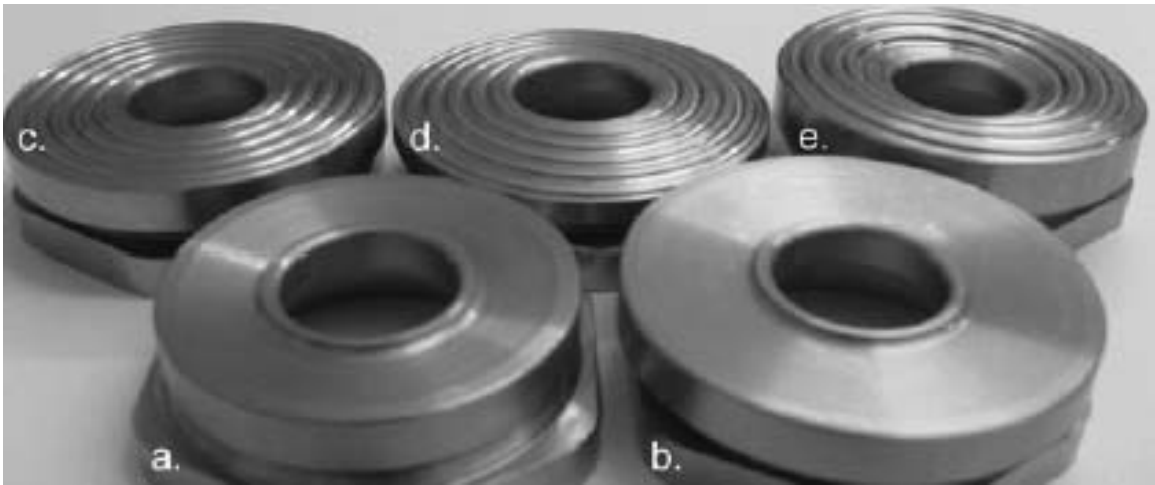
Figure 2-1: Existing Shoulder Geometries [2]

The overall shape of the probe varies from a cylinder to a truncated cone, with several different combinations of threads, flats or flutes as shown in Figure 2-2. Figure 2-3 shows a Trivex^{TM} which uses a three sided probe.

Figure 2-2: Existing Probe Geometries [3]

Figure 2-3: Trivex^{TM} Tool [4]

The tool that BYU currently uses for most welds in aluminum and steel has a convex scrolled shoulder, and the probe is a conical shape with a step spiral. This type of tool is commonly referred to as a CS4 tool (Convex scrolled shoulder, step spiral). A typical CS4 tool is shown in Figure 2-4.

One of the benefits of the CS4 tool over other tool profiles is that the CS4 tool plunges perpendicular to the surface of the workpiece as it traverses the weld. Other tools require a tilt angle which increases the difficulty in running non-linear welds. Another advantage to the CS4 tool is that the process forces in the direction of the weld are significantly decreased.
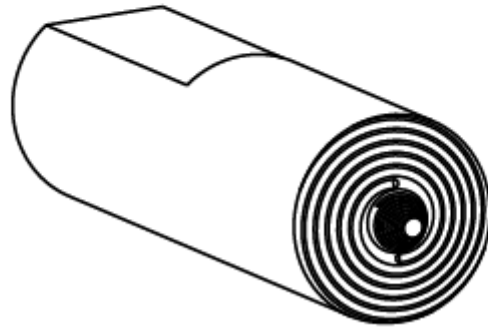
Figure 2-4: CS4 Tool

3 CS4 Tool Geometry

As can be seen in Figure 2-4, the geometry of a CS4 tool is fairly complex. In addition to the pin and shoulder geometry, there are a number of parameters that determine the geometry of the CS4 tool. For clarity (and to reflect typical manufacturing processes), the geometry of the CS4 tool is decribed in steps. First the overall geometry of the CS4 tool is defined, which might be considered the geometry of a CS4 tool with neither a scroll on the shoulder nor a spiral on the pin. The geometry of the tool features are described next, namely the scroll and the spiral. To narrow the range of possible tool geometries, a few simple assumptions have to be made and the descriptions of these assumptions are presented with their corresponding geometries.

3.1 Overall Geometry

3.1.1 Probe Geometry

The probe for the CS4 tool is in the form of a truncated cone, and has three parameters. These are l_p, the probe length; r_p, the radius of the probe at the root of the pin; and φ_p, the half-angle of the cone of the probe.
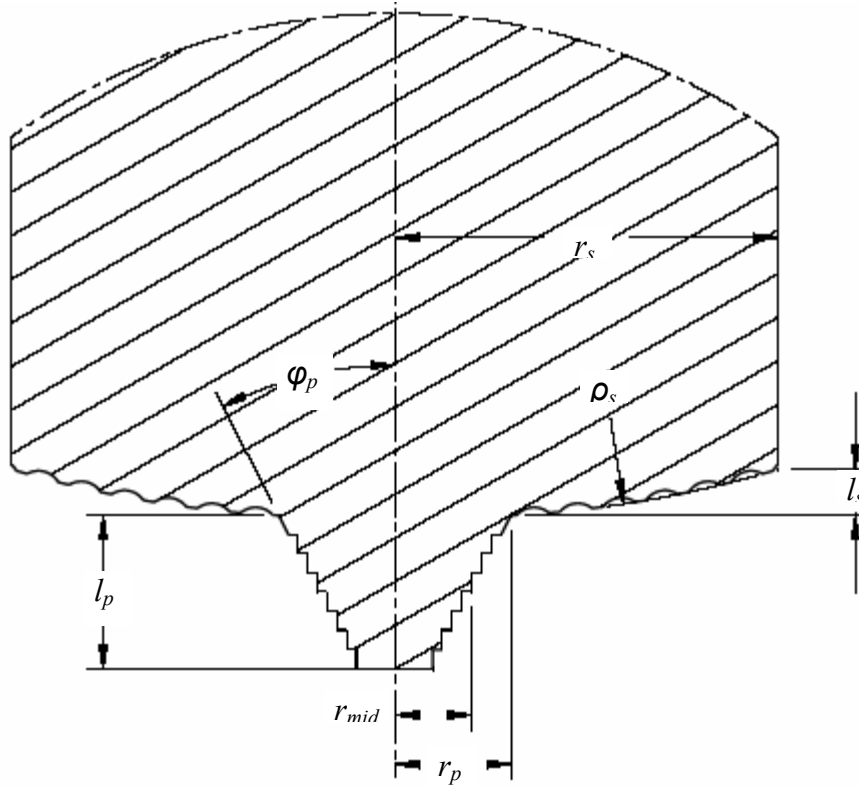
Figure 3-1: Overall Geometry

Throughout this study the probe length, l_p, is held constant at 5.1mm (.200 in). One of the main reasons for holding the probe length constant is so that the plate thickness of the weld material doesn't have to be varied.

For the pilot study the probe root radius was defined as a function of the radius of the end of the probe, r_e, which was held constant at 0.8mm (.030in):

$$r_p = r_e + l_p \tan(\varphi_p)$$ (3-1)

After completion of the pilot study, probe failure on one of the tools prompted a change in the function of the probe root radius. Instead of holding the probe end radius constant, the radius of the probe midway between the end and root, r_{mid}, was held constant and the probe root radius was defined as:

$$r_p = r_{mid} + \frac{l_p}{2}\tan(\varphi_p)$$ (3-2)

The probe mid radius was held at 2.5mm (.100in) for the screening experiment, but because of failure was increased to 2.8mm (.110in) for the composite design. The half-angle of the probe cone, φ_p, is one of the features that is varied throughout this study.

3.1.2   Shoulder Geometry

The shoulder is assumed to be a convex circular arc from the root of the probe to the outer edge of the tool. This is not a requirement for CS4 tools, but is a common feature of the family of tools used in this study. Note that this does not mean that the shoulder is a portion of a sphere. Instead, the shoulder geometry is a revolution of a circular arc around the tool axis.

The shoulder profile has three parameters. r_s is the outer radius of the shoulder (as measured from the tool axis). l_s is the length of the shoulder from the root of the pin to the outer radius, as measured parallel to the tool axis. And ρ_s is the radius of the circular arc that defines the shoulder. The outer radius of the shoulder, r_s, remains constant at

12.6mm (.498in) so that it fits into the tool holder on the FSW machine. The other two parameters are varied throughout this study.

Using the shoulder and probe geometric features, it will become necessary to find the centerpoint of the shoulder radius as a reference point for the scroll cuts on the shoulder. These coordinates are in Cartesian coordinates and there will be only an axial and radial component since the shoulder radius is axially symmetric. To simplify the equations it is helpful to define two intermediate variables; the linear distance, s, between the points where the shoulder meets the probe and where the shoulder meets the outer radius and the angle, λ, between the tool axis and the line that passes through the shoulder radius centerpoint and intersection of the shoulder with the probe (a negative angle means that the radius of the centerpoint is less than the root radius of the probe):

$$s = \sqrt{l_s^2 + (r_s - r_p)^2} \qquad\qquad (3\text{-}3)$$

$$\lambda = \arcsin\left(\frac{s}{2\rho_s}\right) - \arcsin\left(\frac{l_s}{s}\right) \qquad\qquad (3\text{-}4)$$

The axial coordinate of the centerpoint, z_c, is the axial distance from the end of the probe and the radial coordinate, r_c, is the distance from the axis to the centerpoint as shown in Figure 3-2. Note that the radial coordinate could be negative, meaning that the centerpoint is on the opposite side of the axis from the shoulder it defines.

$$z_c = l_p + \rho_s \cos(\lambda) \qquad\qquad (3\text{-}5)$$

$$r_c = r_p + \rho_s \sin(\lambda) \qquad\qquad (3\text{-}6)$$
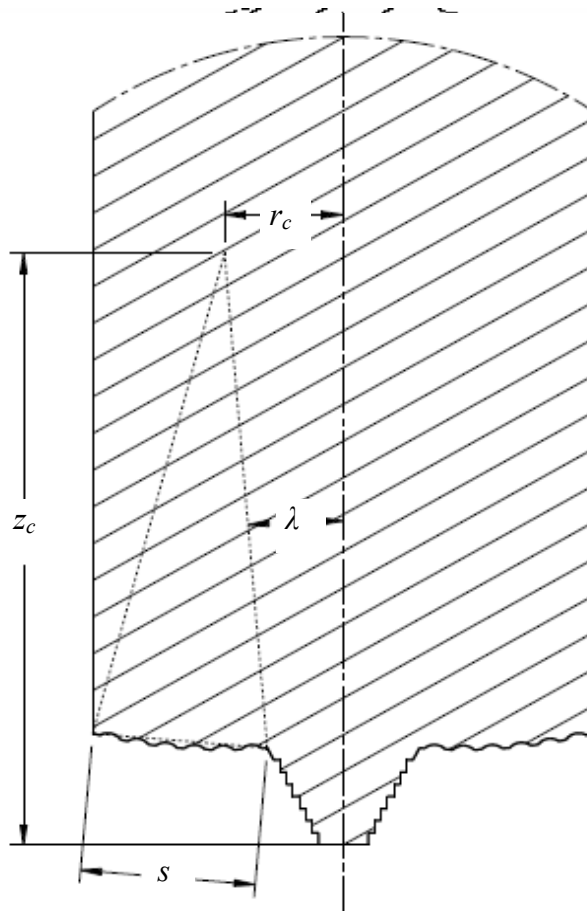
Figure 3-2: Shoulder Radius Centerpoint

3.2 Step Spiral Geometry

The step spiral is a cut out of the truncated cone probe that follows a helical path offset from the surface of the probe. To completely define the geometry of the cut the shape of the cutting tool must be specified, as well as the depth of the cut, the pitch of the cut, and the number of different "starts" associated with the cut, as shown in Figure 3-3.
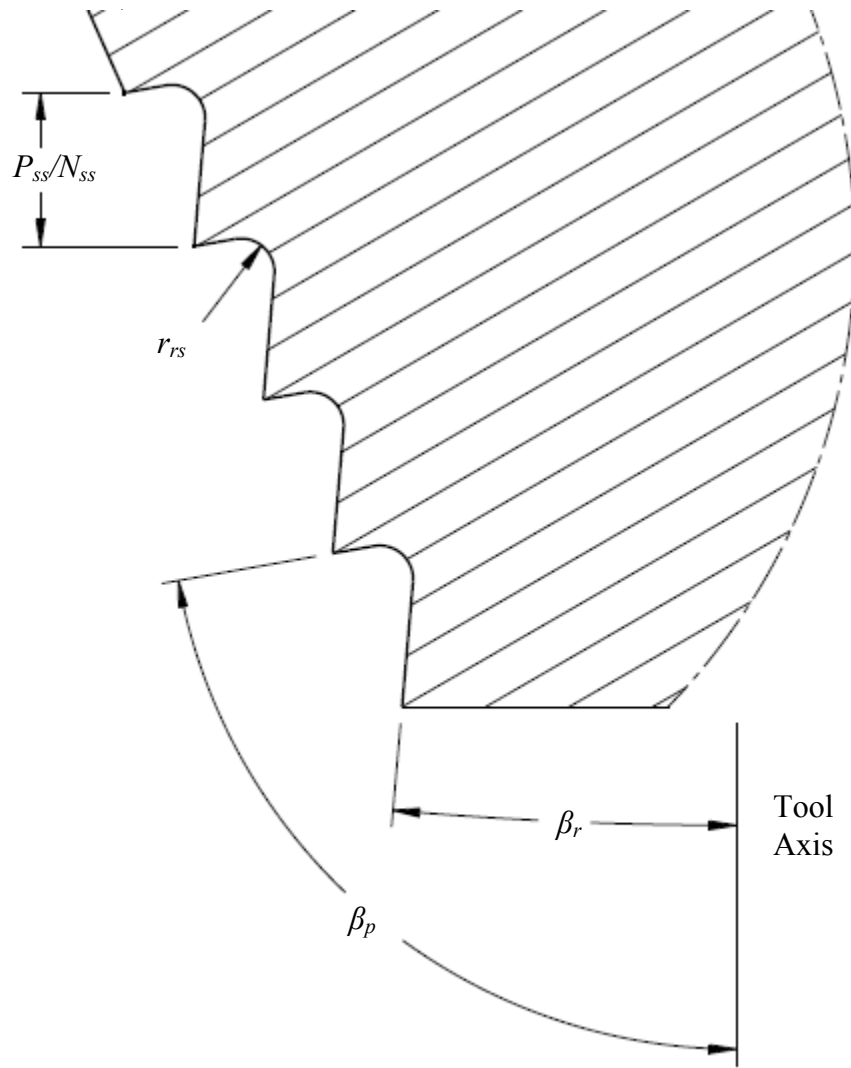
Figure 3-3: Step Spiral Geometry

The shape of the cut region is defined in a plane normal to the helical path of the cut, as shown in Figure 3-3. Borrowing terminology from stairs, each step has a "riser" (a surface roughly parallel to the axis of the tool) and a "tread" (a surface roughly perpendicular to the axis of the tool. The pressure angle of the step spiral, β_p, is the angle between the tread and the tool axis. The relief angle of the step spiral, β_r, is the angle

between the riser and the tool axis. The radius between the stair and the tread is known as the root radius for the spiral, r_{rs}. For the purposes of this study and for simplicity of manufacture, β_p is constant at 90°, β_r is constant at 0°, and r_{rs} is defined to be as close to zero as possible to machine.

With the cut region defined, the shape of the spiral can be defined, as shown in Figure 3-3. The depth of the spiral, d_{ss}, is the distance from the surface of the cone to the intersection of the tread and the riser, measured perpendicular to the tool axis. Note that for a root radius value other than zero, this intersection will be internal to the probe of the tool, rather than on the surface of the spiral cut. The pitch of the spiral, P_{ss}, is the distance between successive treads, as measured parallel to the tool axis. The number of "starts" or "flights" in the step spiral to is the number of different cuts taken to create the spiral. This parameter, N_{ss}, is freely selected. By convention, however, the different starts are spaced equally around the probe, and the start of the spiral is defined to be at the end of the probe, moving toward the root of the probe.

For this study, the spirals are defined such that the angle of the cone shaped probe is not altered and there are no gaps between treads and risers. Therefore, the depth of the spiral is defined as:

$$d_{ss} = \frac{P_{ss}}{N_{ss}} \tan(\varphi_p) \tag{3-7}$$

The pitch of the spiral, P_{ss}, and the number of starts, N_{ss}, are varied through different experiments in this study.

The step spiral is generated by sweeping the cut shape along the spiral, with the intersection of the tread and riser surfaces lying on the spiral. For convenience the spiral

is defined in cylindrical coordinates as a parametric function of ω. ω will range from 0 to ω_f, where:

$$\omega_f = \frac{4\pi}{N_{ss}} + \frac{.9l_p - \dfrac{P_{ss}}{N_{ss}}}{P_{ss}}$$

(3-8)

The radial component of the spiral, $r(\omega)$ is:

$$r(\omega) = \begin{cases} r_p - l_p\tan(\varphi_p); & 0 \le \omega \le \dfrac{2\pi}{N_{ss}} \\[3mm] [r_p - l_p\tan(\varphi_p)] + d_{ss}N_{ss}\dfrac{\omega - \dfrac{2\pi}{N_{ss}}}{2\pi}; & \dfrac{2\pi}{N_{ss}} \le \omega \le \omega_f \end{cases}$$

(3-9)

The axial component of the spiral, $z(\omega)$, starting at the probe end, is:

$$z(\omega) = \begin{cases} P_{ss}\dfrac{\omega}{2\pi}; & 0 \le \omega \le \omega_f - \dfrac{2\pi}{N_{ss}} \\[3mm] .9l_p; & \omega_f - \dfrac{2\pi}{N_{ss}} \le \omega \le \omega_f \end{cases}$$

(3-10)

3.3   Shoulder Scroll Geometry

The cross-section of the scroll geometry is circular, with a radius r_{sc}. In practice, the scroll is cut with a ball-end mill, so for deeper scrolls, the cross section will not be circular. However, for the scrolls used in this study, the circular cross-section applies. This scroll radius is varied though the experiments.

The depth of the scroll is chosen in order to give a specific pressure angle, γ_p, at the intersection between the scroll and the shoulder surface, as shown in Figure 3-4. So that the scroll passes are evenly spaced along the shoulder, they are defined by the

16

centerpoint of the shoulder radius and the angle, α_{sc}, between passes. The number of scrolls is given by N_{sc}. As in the case of the step spiral, multiple scrolls are chosen to be equidistant from each other around the axis of the tool, so they are uniformly spaced on the shoulder.
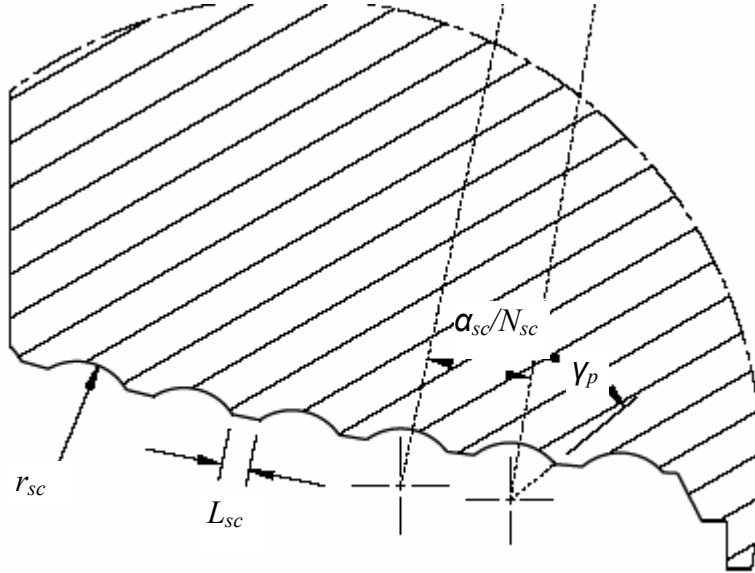
Figure 3-4: Shoulder Scroll Geometry

The pressure angle of the scroll cut, γ_p, is varied at different points in this study, as is the number of scrolls, N_{sc}. The angle between scroll passes, α_{sc}, is defined as a function of a new variable, L_a, which is the fraction of the shoulder area that has not been removed by scroll cuts. L_a can best be visualized using L_{sc} from Figure 3-4. This land fraction is varied during different experiments.

$$L_a = \frac{N_{sc} \, \arcsin\left(\dfrac{L_{sc}}{\rho_s}\right)}{\alpha_{sc}} \qquad \text{(3-11)}$$

17

$$\alpha_{sc} = 2\arcsin\left[\frac{\left(1+\frac{L_a}{1-L_a}\right)r_{sc}N_{sc}\sin(\gamma_p)}{\rho_s}\right]$$ **(3-12)**

Like the step spiral, the scroll cuts are also defined in Cartesian coordinates. The path of the function defines where the centerpoint of the scroll radius, r_{sc}, passes. This time the axial and radial components will vary as a function of θ, beginning with θ equal to zero and increasing until the scroll has passed the outer radius of the tool.

$$z(\theta) = z_c - \left[\rho_s + r_{sc}\sin\left(\frac{\pi}{2}-\gamma_p\right)\right]\cos\left[\frac{\theta}{2\pi}\alpha_{sc} - \arcsin\left(\frac{r_s - r_p - r_{sc}}{\rho_s}\right)\right]$$ **(3-13)**

$$r(\theta) = r_c + \left[\rho_s + r_{sc}\sin\left(\frac{\pi}{2}-\gamma_p\right)\right]\sin\left[\frac{\theta}{2\pi}\alpha_{sc} - \arcsin\left(\frac{r_s - r_p - r_{sc}}{\rho_s}\right)\right]$$ **(3-14)**

3.4 Geometric Features to be Studied

Overall there are nine different geometric features that have been chosen as possible factors in this study. The nine features and their corresponding variables are shown in Table 3-1.

Table 3-1: Nine Geometric Features for Study

Description	Variable
Cone Half-Angle of the Probe	φ_p
Shoulder Radius	ρ_s
Shoulder Length	l_s
Number of Step Spiral Starts	N_{ss}
Pitch of Step Spiral	P_{ss}
Scroll Pressure Angle	γ_p
Number of Scroll Starts	N_{sc}
Scroll Radius	r_{sc}
Scroll Land Fraction	L_a

4 Pilot Study

The CS4 tool designs used in this study were slightly different from those used in previous work. For example, the shoulder convex radius, ρ_s, was much smaller than previous tools, which created the possibility that the lowest point on the shoulder in the axial direction could extend beyond the point where the shoulder meets the probe as shown in the tool in Figure 4-1a. This type of geometry had not been tried before. In addition, the cross sectional geometry of the scroll was a circular arc as shown on the tool in Figure 4-1b, rather than a complex geometry developed by using an angled grinding wheel to shape the scroll as shown on the tool in Figure 4-1c. Because these design differences might lead to process failure or tool failure, it was determined that a pilot study should be performed to explore the performance of these tools and give guidance for the statistical screening design.

a   b   c
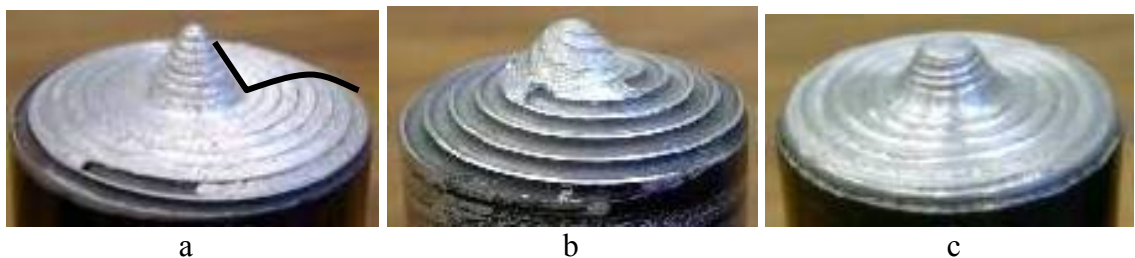
Figure 4-1: Pilot Study Exploration

4.1 Pilot Study Design

A pilot study was developed using five tools, each of which had at least one parameter that varied significantly from the nominal design which was created. The parameters that were chosen to be varied in this pilot study were those that seemed to have the greatest likelihood of producing process failure or tool failure. The parameters that were held constant in the pilot study are listed in Table 4-1. The values for each of the variable parameters in the pilot study are listed in Table 4-2.

Table 4-1: Constant Tool Parameters for the Pilot Study

Parameter	Value	Parameter	Value
P_{ss}/N_{ss}	.63 mm (.025 in)	N_{sc}	2
γ_p	60 deg	L_a	1/3

Table 4-2: Variable parameters for the Pilot Study

Tool	Probe Cone Angle	Shoulder Length	Step Spiral Starts	Scroll Radius	Shoulder Radius
	φ_p, deg.	$l_{s,}$, mm(in)	N_{ss}	r_{sc}, mm (in)	ρ_s, mm (in)
1	40°	1.6 (0.063)	2	12.7 (0.5)	25.4 (1)
2	20°	1.6 (0.063)	2	12.7 (0.5)	25.4 (1)
3	30°	1.6 (0.063)	2	12.7 (0.5)	11.3 (0.444)
4	30°	3.2 (0.126)	2	12.7 (0.5)	25.4 (1)
5	30°	1.6 (0.063)	4	19.1 (0.75)	25.4 (1)

Tool 1: Large Φ_p Tool 2: Small Φ_p Tool 3: Small ρ_s

Tool 1-4: $N_{ss} = 2$

Tool 5: $N_{ss} = 4$

Tool 4: Large l_s Tool 5: Large r_{sc}
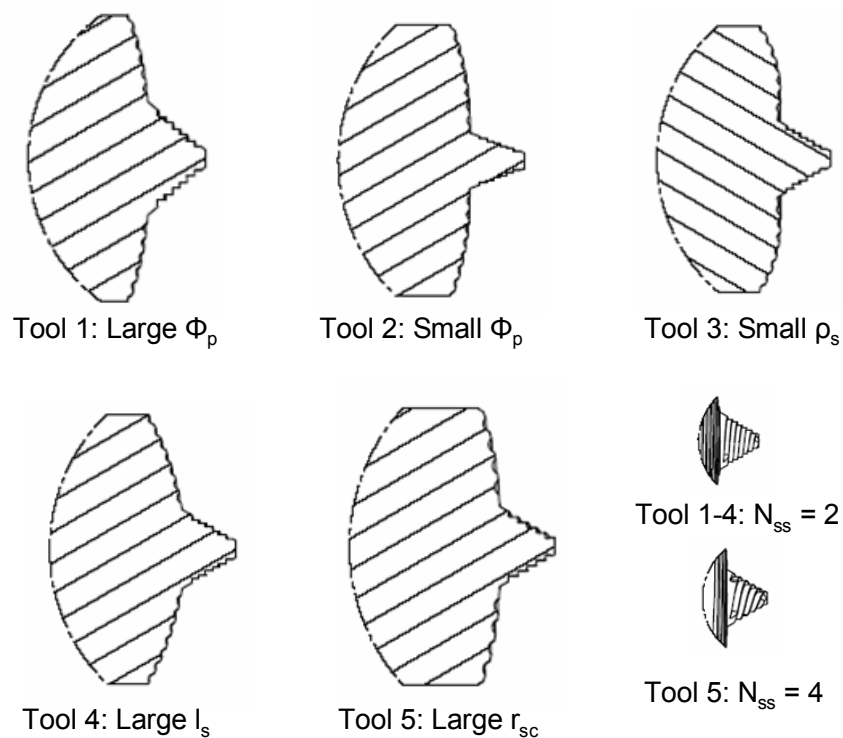
Figure 4-2: Tool Profiles for Pilot Study

The tools for the pilot study were run at a range of parameters that had been successful with the previous CS4 tools, in order to make comparisons with earlier work. Pew et al. [5] had previously run CS4 tools at feed rates from 126-280 mm/min (5-11 ipm) and spindle speeds of 200-800 rpm. To test the tools at a variety of combinations of these parameters each tool was used to make three different welds at fixed feed rates of 126 mm/min (5 ipm), 203 mm/min (8 ipm), and 280 mm/min (11 ipm). In each of these welds the spindle speed would start at 200 rpm. When process loads maintained a steady state, the spindle speed was increased to 500 rpm. Once steady state was reached, the

23

spindle speed was increased to 800 rpm. Axial, longitudinal, and transverse forces and spindle torques were measured during each of the steady-state periods.

Welds in the pilot study were run in position control mode. Depths were chosen to engage the same percentage of the tool shoulder for all the welds. Because the shoulder geometries were significantly different, different tools required different depths to achieve the same width of weld. In order to find the appropriate depths, a few practice welds were run to find the depth that produced a weld width approximately 75-80% of the diameter of the tool. Tools 1, 2 and 5 were run at 6.0 mm (.235 in) plunge; Tool 3 was run at 5.5 mm (.215in) plunge; and Tool 4 was run at 7.0 mm (.275in) plunge.

4.2   Pilot Study Results

The tools were able to produce welds at most combinations of parameters. Some of the parameters left considerable amounts of flash and there was a wide range of surface finish quality for each of the welds.

The narrow probe on Tool 2 broke off early in the 280 mm/min (11 ipm) weld due to the process forces. Tool 2 is the second from the left in Figure 4-3 and can be seen after the probe sheared off. The broken probe was not totally unexpected, due to the small diameter. However, it does mean that the Tool 2 force results for the 280 mm/min weld are not representative of the process and should probably be ignored. In the future, tools with probes as narrow as Tool 2 will not be used. The data for Tool 2 is included in the results for the forces and torques, but it should be noted that the values at high feed rates are skewed because of the broken pin.
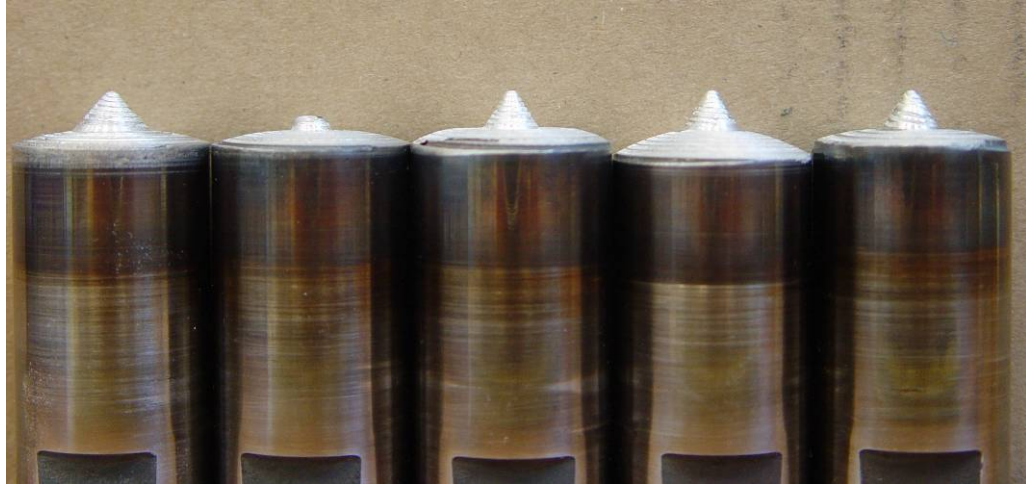
Figure 4-3: Pilot Study Tools After Use

In order to define the forces better, a coordinate system is defined as shown in Figure 4-4. The axial force is in the Z direction. The longitudinal force is in the X direction and the lateral force is in the Y direction. Because of sign convention and the rotational direction of the spinning tool, the lateral force is negative for all welds.
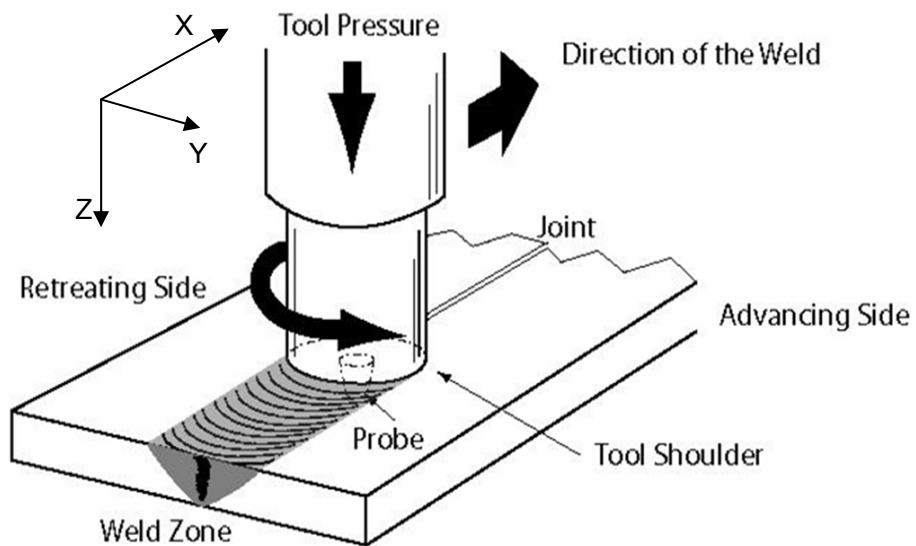
Figure 4-4: Coordinate System

Figure 4-5 shows that as expected, the axial force (Z load or Forge load) increased with feed rate. A few exceptions were Tool 1 which showed a decrease in axial load at the fastest travel speed and Tool 5 which had an elevated axial load at the slowest travel speed for the slowest spindle speed.
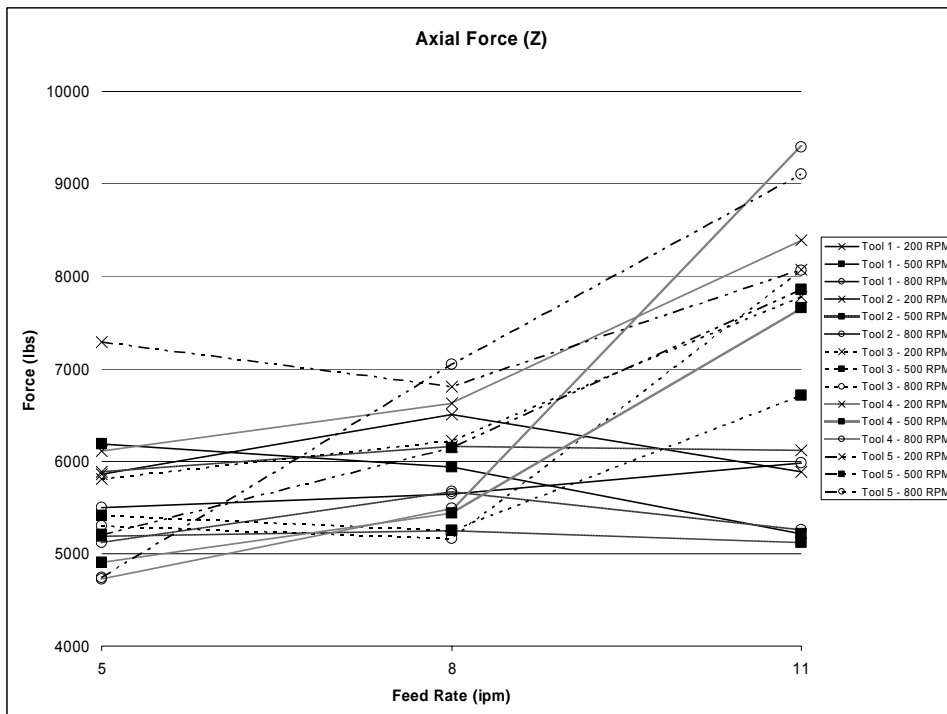
Figure 4-5: Axial Force vs. Feed Rate

Figure 4-6 shows that for most of the welds, axial force decreased with an increase in spindle speed from 200 to 500 rpms and then stayed constant between 500 and 800 rpms. However, some tools showed increased axial forces at 800 rpms when run at fast travel speeds.

26

Axial Force (Z)

Force (lbs) vs Spindle Speed (RPM)

Legend:
- Tool 1 - 5 ipm
- Tool 1 - 8 ipm
- Tool 1 - 11 ipm
- Tool 2 - 5 ipm
- Tool 2 - 8 ipm
- Tool 2 - 11 ipm
- Tool 3 - 5 ipm
- Tool 3 - 8 ipm
- Tool 3 - 11 ipm
- Tool 4 - 5 ipm
- Tool 4 - 8 ipm
- Tool 4 - 11 ipm
- Tool 5 - 5 ipm
- Tool 5 - 8 ipm
- Tool 5 - 11 ipm
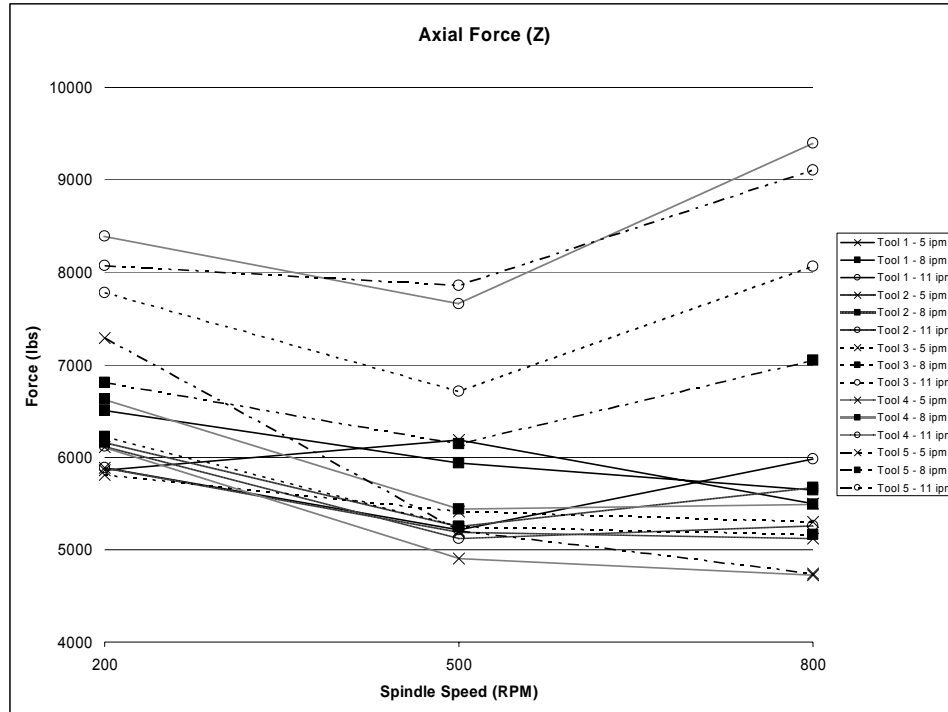
Figure 4-6: Axial Force vs. Spindle Speed

For most welds and tools, longitudinal force decreased from 200 to 500 rpms and then remained steady as spindle speed increased to 800 rpms as shown in Figure 4-7. This is the expected result due to increased heat generation. However, at the highest weld speed of 280 mm/min (11 ipm), longitudinal force increased between 500 and 800 rpms for some of the tools.

As expected, longitudinal force increased with feedrate for all tools and spindle speeds as can be seen in Figure 4-8. Tool 4 at 800 rpm showed a dramatic increase in longitudinal force at 280 mm/min when compared to the other tools.

27
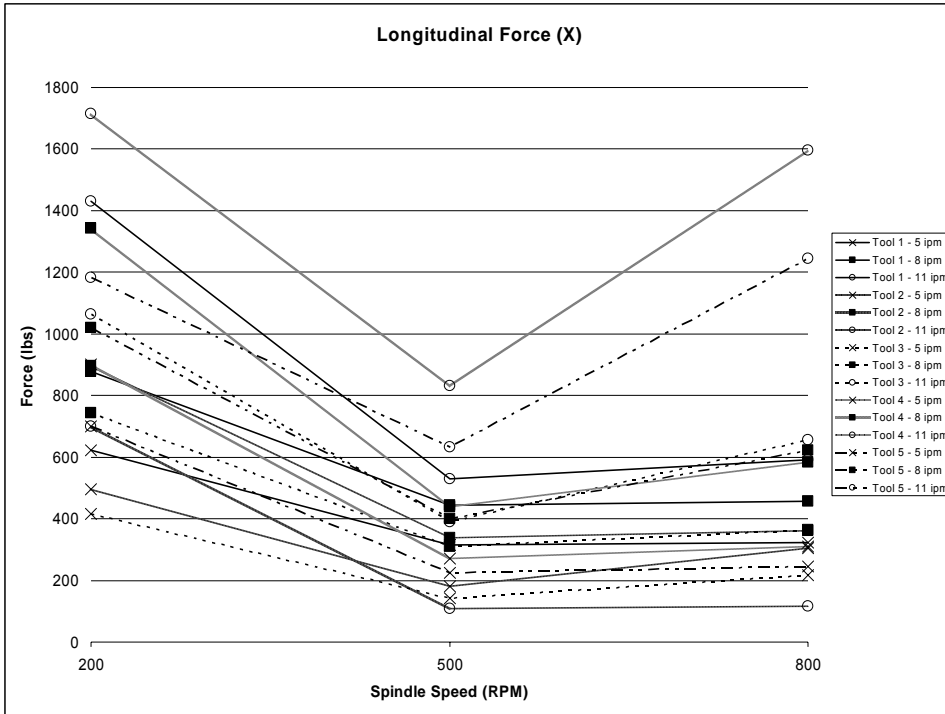
Figure 4-7: Longitudinal Force vs. Spindle Speed
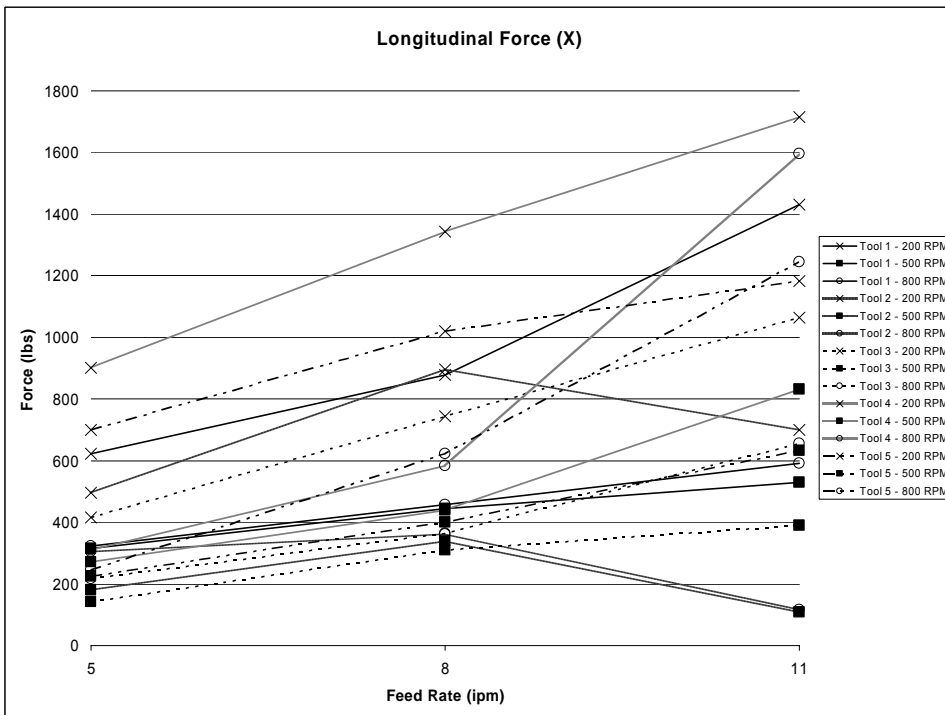
Figure 4-8: Longitudinal Force vs. Feed Rate

28

For all of the welds in the pilot study, the lateral force was negative. In this discussion, lateral forces will be considered to increase when the magnitude of the lateral force increases. Every tool and feed rate setting studied shows a minimum in the lateral force at a spindle speed of 500 rpm as shown in Figure 4-9. This minimum in the lateral force provides an interesting data point for future fundamental studies.

In contrast, most tools show an increase in the magnitude of the lateral force as feed rate increases. At intermediate feed rates, tools 2 and 3 show a minimum in the magnitude of the lateral force.
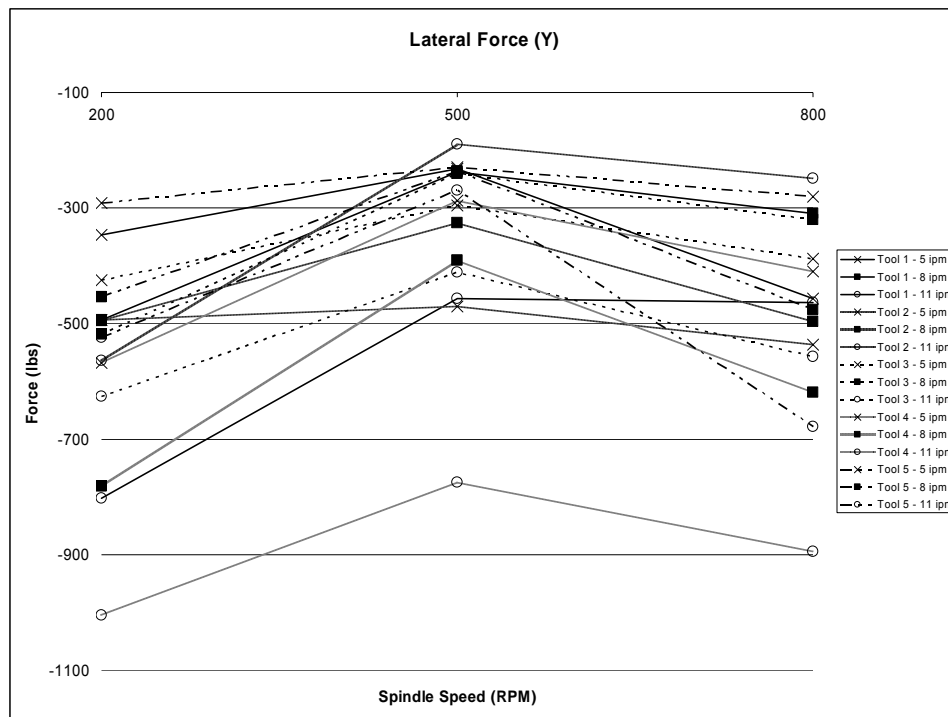
Figure 4-9: Lateral Force vs. Spindle Speed
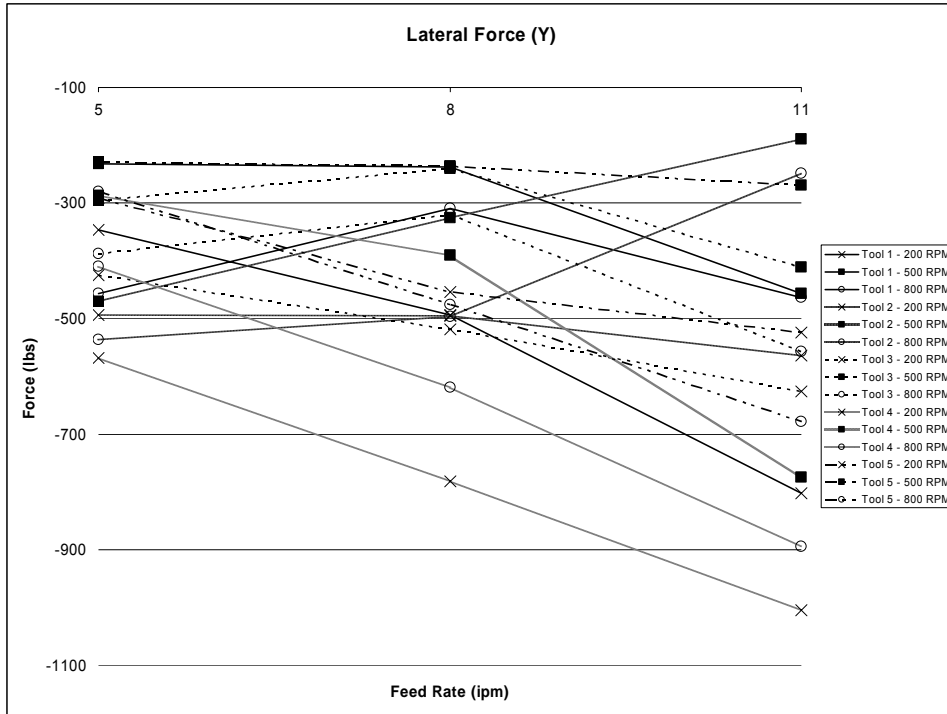
Figure 4-10: Lateral Force vs. Feed Rate

In most cases, as expected, spindle torque increases decreases as spindle speed increases. This result is shown in Figure 4-11. However, tool 5 shows a minimum in spindle torque at 500 rpm when the feed rate is 280 mm/min.

For most of the tools the spindle torque is not affected greatly by the feed rate as shown in Figure 4-12. Most of the tools show a slight increase in torque for higher feed rates, but it isn't a steep incline. Tool 3 at a spindle speed of 800 rpm shows a minimum in spindle torque at a feed rate of 203 mm/min.

30
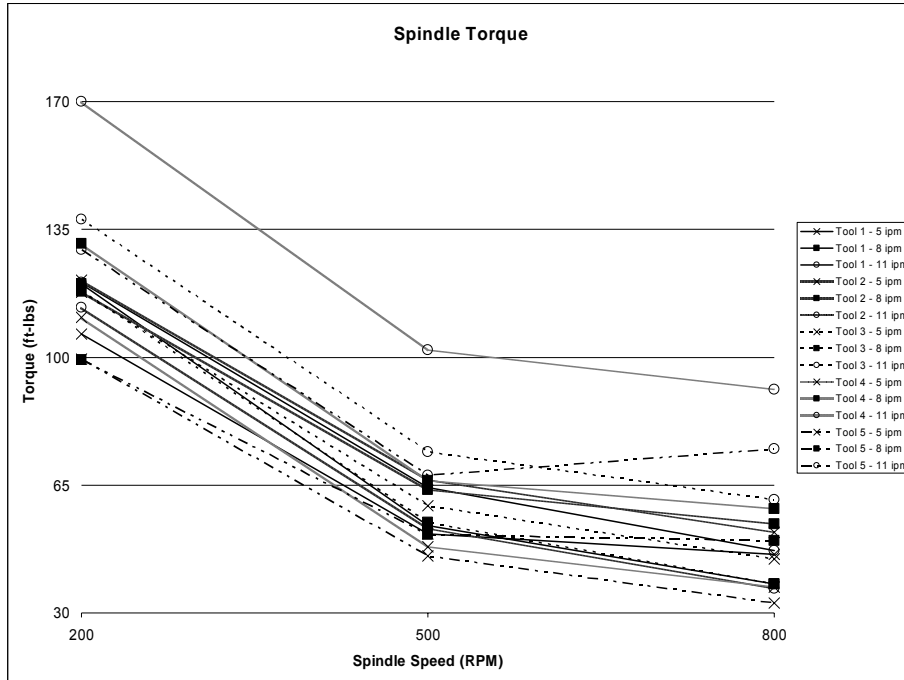
Figure 4-11: Spindle Torque vs. Spindle Speed
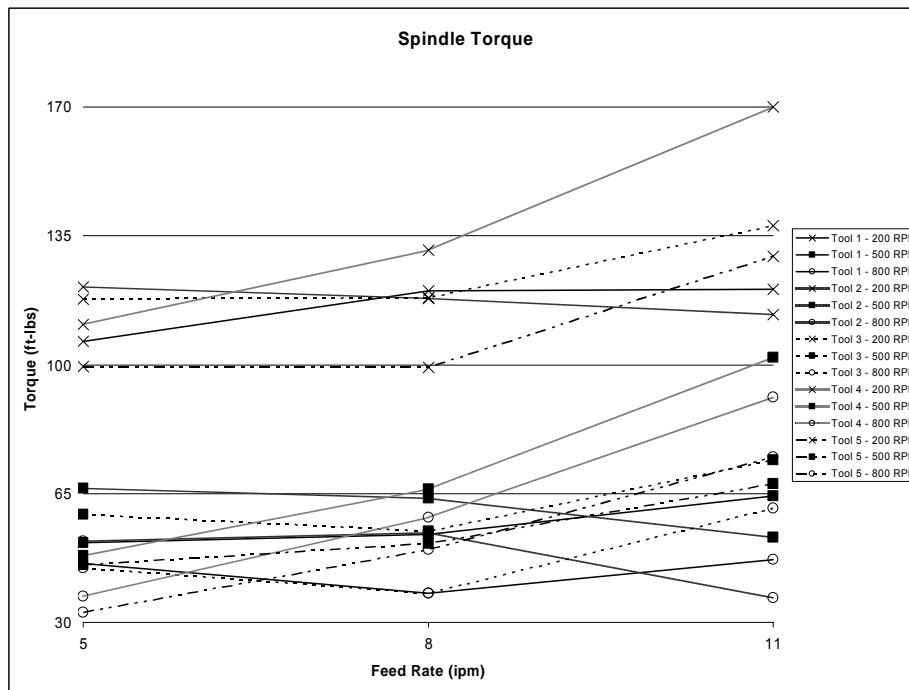
Figure 4-12: Spindle Torque vs. Feed Rate

31

4.3   Pilot Study Discussion of Results

All of the tools were able to produce fully consolidated welds. Some of them performed better at higher or lower feed rates and spindle speeds, but all of them produced quality welds at one or more combinations of process parameters. Tool 4 had the highest forces and torques while Tool 1 had the lowest forces and torques, showing that there is sufficient variation in the forces and torques between tools to warrant further investigation of the significance of geometric features.

The other purpose of the pilot study was to determine if any of the tool features would lead to process failure or tool failure. There was no process failure for any of the weld parameters. There was one tool failure. Almost the entire probe on Tool 2 sheared off at the high feed rate. Therefore the probe diameter was insufficient for the process forces and will have to be increased for further study.

Altogether, the pilot study demonstrated that a wide variety of CS4 tools would produce sound welds over a range of parameters and increased the confidence that a bold experimental plan could be successful.

5   Screening Experiment

5.1   Screening Experimental Design

The next step was to determine which tool design parameters have the greatest influence on the response variables and quantify those relationships.   A modified Plackett-Burman screening experiment [6] was chosen, because it allows the exploration of up to 11 factors with only 12 tools. The only disadvantage is that the two-way interactions are confounded with the main effects. A design that would have two-way interactions clear of main effects would require too many (32) different tools.

Table 5-1 shows the variable parameters used in the screening design, along with the low, high and center values of each of these parameters. Table 5-2 lists the variable settings for each of the factors for each run of the experimental design, which consists of a 12-run Plackett-Burman design plus an additional center point, for a total of 13 runs. The high, low and center values are represented with a 1, -1 or 0, respectively.

Since the probe sheared off of Tool 2 in the pilot study, the formula for calculating the probe radius at the root was modified as described in 3.1.1. The variables that were included in the screening experiment are shown in Table 3-1.

33

Table 5-1: Factor Levels for Each Variable in Screening Experiment

Factor	Variable	Symbol	Units	Low	Center	High
X1	Probe Cone Angle	$\varphi_p{'}$	deg	15	25	35
X2	1/Shoulder Radius	$1/\rho_s$	mm^{-1} (in^{-1})	0.020 (0.5)	0.040 (1)	0.060 (1.5)
X3	Shoulder Length	l_s	mm (in)	1.5 (0.06)	2.3 (0.09)	3.0 (0.12)
X4	Step Spiral Starts	N_{ss}		2	3	4
X5	SS Starts/SS Pitch	N_{ss}/P_{ss}	mm^{-1} (in^{-1})	0.79 (20)	1.37 (35)	1.97 (50)
X6	Scroll Pressure Angle	γ_p	deg	45	60	75
X7	Scroll Starts	N_{sc}		2	3	4
X8	Scroll Radius	r_{sc}	Mm (in)	0.5 (0.02)	0.63 (0.025)	0.75 (0.03)
X9	Scroll Land Fraction	L_a		0.25	0.375	0.5

Table 5-2: Plackett-Burman Experimental Design

Tool	X1	X2	X3	X4	X5	X6	X7	X8	X9
1	1	1	-1	1	1	1	-1	-1	-1
2	1	-1	1	1	1	-1	-1	-1	1
3	-1	1	1	1	-1	-1	-1	1	-1
4	1	1	1	-1	-1	-1	1	-1	1
5	1	1	-1	-1	-1	1	-1	1	1
6	1	-1	-1	-1	1	-1	1	1	-1
7	-1	-1	-1	1	-1	1	1	-1	1
8	-1	-1	1	-1	1	1	-1	1	1
9	-1	1	-1	1	1	-1	1	1	1
10	1	-1	1	1	-1	1	1	1	-1
11	-1	1	1	-1	1	1	1	-1	-1
12	-1	-1	-1	-1	-1	-1	-1	-1	-1
13	0	0	0	0	0	0	0	0	0
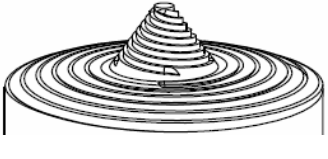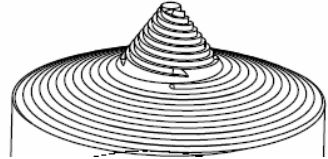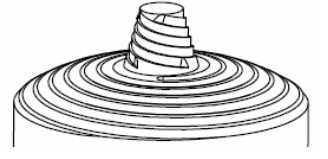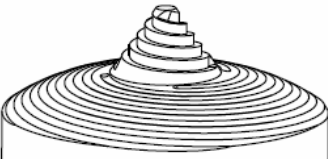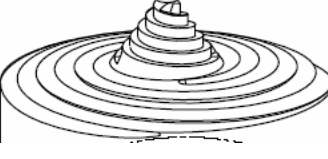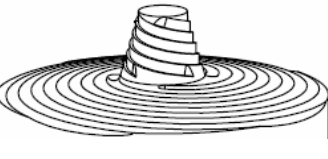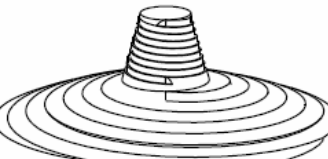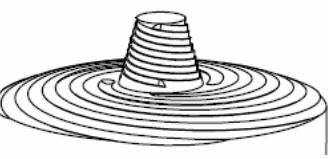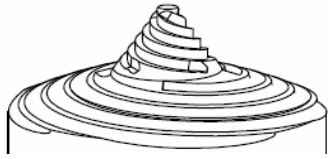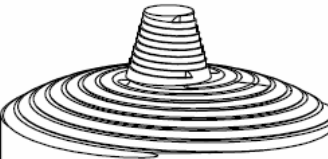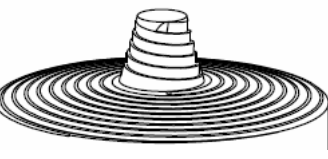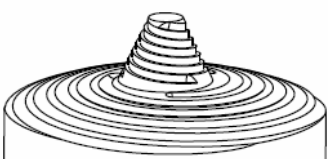
PB01	PB02	PB03
PB04	PB05	PB06
PB07	PB08	PB09
PB10	PB11	PB12
PB13		

Figure 5-1: Screening Experiment Tools

One observation from the pilot study was that the worst welds (poor surface finish or high forces) were the welds run at high spindle speed and low travel speed, or welds

run at low spindle speed and high travel speed. To reduce this effect it was determined that each tool would be run at two fixed feed rates; at 152 mm/min (6 ipm) and at 254 mm/min (10 ipm). In the pilot study, each weld would consist of three different spindle speeds with enough time to reach a steady state at each spindle speed. The difference between the screening experiment and the pilot study is that a variation of a Pseudo Heat Index (PHI) proposed by Chimbli et al. [7] would be used to vary the spindle speeds (Chimbli's equation includes an effective pin length).

$$PHI = \frac{(RPM)^2}{IPM}$$ (5-1)

Instead of running the welds at the same combination of spindle speeds for each feed rate, the PHI would stay the same so that the welds run at higher travel speeds would be run at higher spindle speeds as shown in Table 5-3.

Table 5-3: Spindle Speeds for Screening Experiment

Travel Speed	Spindle Speeds (RPM)		
mm/min (ipm)	Low	Medium	High
152 (6)	259	433	606
254 (10)	335	559	782

In the pilot study, the welds were run at different plunge depths to achieve the same width of weld. For the screening experiment it was determined that plunge depth would be one of the factors investigated. It was determined that the welds would be run at

a plunge depth equal to the probe length (constant for all tools) plus a fraction (f_p) of the shoulder length (l_s).

$$plunge\,depth = l_p + f_p * l_s \qquad\qquad \textbf{(5-2)}$$

Three different plunge depths were desired for each tool. The plunge fractions and their corresponding plunge depths for the different shoulder lengths are shown in Table 8. Therefore, one weld was run at each plunge depth for the two travel speeds for a total of six welds with each tool. Since each weld has three different spindle speeds, there is a total of 18 different weld parameters for each of the 13 tools created.

Table 5-4: Plunge Depths for Screening Experiment

Plunge fraction, f_p	.4 (Low)	.55 (Medium)	.7 (High)
l_s = 1.5 mm (.06 in)	5.7 mm (.224 in)	5.9 mm (.233 in)	6.1 mm (.242 in)
l_s = 2.3 mm (.09 in)	6.0 mm (.236 in)	6.3 mm (.250 in)	6.7 mm (.263 in)
l_s = 3.0 mm (.12 in)	6.3 mm (.248 in)	6.7 mm (.266 in)	7.2 mm (.284 in)

The tools each contained a thermocouple hole, where a Type K Thermocouple was inserted along the axis up to the root of the probe. Figure 5-2shows the thermocouple hole for a typical tool. After each of the welds had achieved a steady state, the average values of the forces, torques and temperatures were measured and used as the yield for the screening experiment analysis.
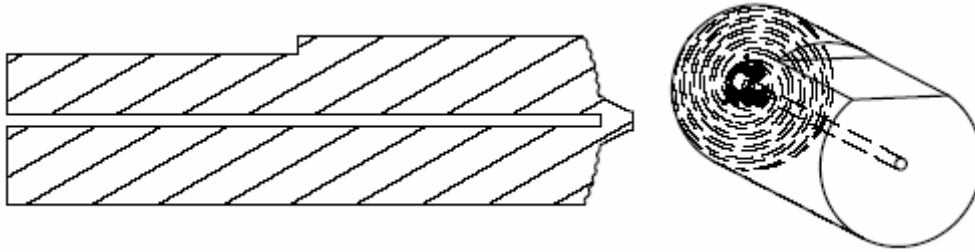
Figure 5-2: Cross-section and Isometric Views of Thermocouple Hole

5.2   Screening Experiment Results

Each of the tools was used for a practice weld before actually running the welds that would be used to record data. During these practice welds, three of the tools lost the tips of their probes because of the longitudinal force of the weld. These three tools were Tools 4, 5, and 10. The common thread in these tools is that they had a large cone angle on the probe and also large risers for the step spiral on the probe. The combination of these two factors left a long skinny portion of probe at the very tip. The three tools all broke at the same spot, within .03mm (.001 in) of each other. To accommodate the broken probes, the plunge depths were adjusted so that the shoulders of the tools would engage the same amount of weld material as the other tools with similar shoulder profiles. The only other tool failure was another probe that sheared completely off of Tool 3. The welds performed with Tool 3 prior to the break were included in the analysis.

After all of the welds were completed and the average forces, torques and temperature had been recorded, five different regressions were performed. The variables in the regression were the factor levels for each of the nine geometric features chosen previously (X1-X9), the weld parameters; feed rate (X10), plunge depth (X11), and PHI

(X12), and the two level interactions between the geometric features and each of the weld parameters. The low feed rate was assigned a factor level of -1 and the high feed rate a factor level of 1. The plunge depth and spindle speeds were also assigned levels with -1, 0 and 1 corresponding to the low, medium and high levels respectively. Another variable, X13, was also included to represent Tools 4, 5, and 10 so that there wouldn't be any interference with the results of the regression because of the broken probe tips. Interactions between geometric features could not be investigated because of the constraints of the screening design. The responses for the five different regressions were the axial force, longitudinal force, lateral force, spindle torque and tool temperature.

For the regression, the significance level was chosen to be a p-value of 0.05. Any factors or interactions that did had a p-value lower greater than 0.05 were dropped from the regression. Using the stepwise regression function in Minitab, all of the insignificant variables were eliminated from the five regressions. Table 5-5 shows the coefficients for each of the nine geometric features and for their interactions with the process parameters for each of the five response variables. Only the significant coefficients are shown.

Table 5-5: Significant Coefficients for Screening Experiment

	X				Y				Z				Temp				Torque			
		X10	X11	X12		X10	X11	X12		X10	X11	X12		X10	X11	X12		X10	X11	X12
1	88.9	-18.4	-10.9	-8.9	-60.5	-14.3	-21.6	-2.3	831.6	-77.0	278.4	0.0	356.0	0.0	27.6	17.8	-76.8	0.0	-31.0	0.0
X1	0.0	-5.1	0.0	-2.0	34.7	0.0	0.0	0.0	0.0	0.0	0.0	0.0	0.0	-5.6	0.0	0.0	0.0	-3.7	0.0	-1.1
X2	-17.0	4.4	0.0	5.2	0.0	0.0	0.0	0.0	169.6	24.9	-16.9	0.0	18.2	0.0	-5.2	0.0	-31.8	0.0	5.0	1.4
X3	-25.9	11.5	16.0	6.0	0.0	0.0	-5.8	0.0	-45.0	24.6	42.1	0.0	0.0	3.6	3.0	0.0	0.0	0.0	0.0	1.2
X4	0.0	0.0	0.0	0.0	0.0	0.0	0.0	0.0	0.0	0.0	18.7	0.0	0.0	0.0	0.0	0.0	-6.9	0.0	0.0	0.0
X5	0.0	0.0	0.0	1.4	-17.8	0.0	0.0	-2.1	0.0	0.0	0.0	0.0	0.0	0.0	-1.7	0.0	0.0	0.0	0.0	0.0
X6	0.0	0.0	0.0	0.0	29.1	0.0	-5.5	-6.0	63.8	0.0	-33.2	-9.7	2.8	0.0	0.0	0.0	-15.7	0.0	5.8	2.9
X7	0.0	0.0	0.0	0.0	17.3	0.0	0.0	-3.0	72.4	0.0	-18.9	-12.9	4.9	-4.4	0.0	0.0	-7.6	0.0	0.0	2.5
X8	0.0	0.0	0.0	0.0	8.7	0.0	0.0	0.0	65.2	0.0	0.0	-10.8	0.0	3.5	0.0	0.0	-10.3	0.0	0.0	1.9
X9	0.0	0.0	0.0	0.0	-9.6	0.0	0.0	0.0	0.0	0.0	0.0	0.0	0.0	0.0	0.0	0.0	4.5	-3.3	0.0	0.0

5.3   Screening Experiment Discussion of Results

After completion of the five regression analyses, all nine of the geometric features were significant in one or more of the regressions. The purpose of the regression analysis was to determine which of the nine geometric features were significant for inclusion in a more comprehensive response surface analysis. Based on the results of the screening experiment, all of the nine features have a statistically significant effect on the five response variables and would therefore need to be included for any comprehensive response surfaces. However, it can also be seen that some of the values of the coefficients are much larger than others, signifying that those variables carry more weight in determining the response variables. In order to quantify the impact of each variable on the response variables, the sum of the magnitude of the main effect coefficients with the magnitude of any interactions between that variable and the process parameters is calculated. These sums are shown in Table 5-6. A Pareto diagram in Figure 5-3 also shows these sums normalized by the largest sum, so that the coefficients that have the greatest impact on the response variables can be more easily seen.

Table 5-6: Combined Magnitude of Coefficients

Factor	Variable	Longitudinal Force	Lateral Force	Axial force	Tool Temperature	Spindle Torque
X1	Probe Cone Angle	7.1	34.7	0.0	5.6	4.8
X2	1/Shoulder Radius	26.6	0.0	211.3	23.4	38.2
X3	Shoulder Length	59.4	5.8	111.7	6.6	1.2
X4	Step Spiral Starts	0.0	0.0	18.7	0.0	6.9
X5	SS Starts/SS Pitch	1.4	19.8	0.0	1.7	0.0
X6	Scroll Pressure Angle	0.0	40.7	106.7	2.8	24.4
X7	Scroll Starts	0.0	20.3	104.3	9.3	10.1
X8	Scroll Radius	0.0	8.7	76.0	3.5	12.2
X9	Scroll Land Fraction	0.0	9.6	0.0	0.0	7.8
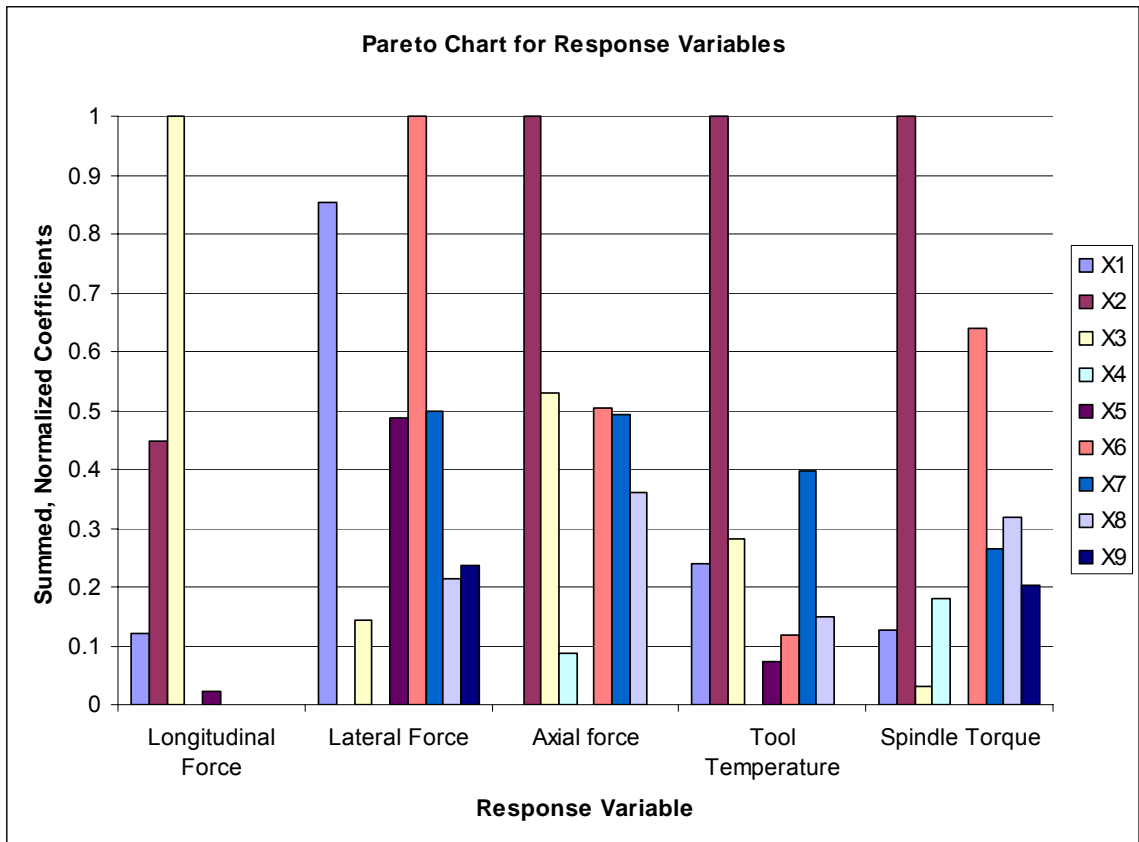
Figure 5-3: Pareto Chart for Screening Experiment

Certain trends can also be detected for some of the variables. For the lateral force (Y), the largest coefficient was the probe cone angle (X1). As the probe cone angle increased, the magnitude of the lateral force decreased. For the axial force (Z), the largest coefficient was 1/shoulder radius (X2). As the shoulder radius was smaller and had more curvature, the axial force increased, probably due to a larger volume of tool that was penetrating the workpiece.

However, many of the effects are not as obvious. For example, a larger shoulder length (X3) decreases the longitudinal force (X); but the interaction effects of increasing

the shoulder length, coupled with increasing any of the process parameter values, increases the longitudinal force. Because there are so many combinations of variables and interaction effects with the process parameters, it is difficult to pinpoint all of the trends for each of the response variables.

5.4   Screening Experiment Conclusions

The benefit of this screening experiment has been to compare the values of the significant coefficients for each of the nine geometric features and their interactions with the process parameters. These values are important in the selection of an appropriate response surface design.

The shoulder radius (X2) was by far the most important geometric feature. It was the largest coefficient for the axial force, the tool temperature and the spindle torque. The shoulder length (X3) is also very important as it was the largest coefficient for the longitudinal force and the second largest for the axial force. The scroll pressure angle (X6) is also important as the largest coefficient for the lateral force and the second largest for the spindle torque. The probe cone angle was very important in determining the lateral force as well. The rest of the variables, though statistically significant, were not as important as these four.

Another benefit of the screening experiment was that it revealed a combination of step spiral pitch and probe cone angle that was insufficient to handle the process forces. It also showed that the probe diameter needs to be increased to avoid further probe breaks.

With these results, it became possible to come up with a central composite design that would adequately model the response surface.

6 Central Composite Experiment

A response surface design involving just seven of the geometric features would require 83 tools for a central composite design. 57 tools would be required for a Box-Behnken design or 40 for a small composite design, neither of which gives as much information as the central composite design. Because of the cost of producing each individual tool, it was determined that only the most important geometric features would be included in the response surface.

After inspecting the coefficients of each of the regressions, as shown in Table 5-6 and Figure 5-3, it was observed that four of the geometric features had much higher effect on the response surface of each of the yields than the other five features. These four were the cone angle of the pin ,φ_p (X1); the radius of curvature on the shoulder, ρ_s (X2); the shoulder length, l_s (X3); and the pressure angle of the scroll cut, γ_p (X6). These four variables are the first and second most important variables for each of the response variables. A central composite design involving four variables only requires 25 tools.

It was also noted that including one more variable to the design only added an additional 2 tools because the design changes from a full to fractional design. Since none of the other variables stood out from the others, a regression was performed to see if any of the variables had a significant effect on the amount of variation in the longitudinal and lateral forces (a possible indicator of poor weld quality). Instead of using the average of

the forces, the standard deviation of the forces was used as the response variable. After calculating the regression coefficients, it was noted that the pitch of the step spirals, P_{ss}, divided by the number of step spirals, N_{ss} (X5) was almost twice as significant as any other variable in increasing or decreasing the amount of variation in both the longitudinal (X) and lateral (Y) forces. Therefore, X5 was also included in the central composite design.

6.1   Central Composite Design

An example central composite design consisting of a two level factorial design with additional star points and centerpoints as shown in Figure 6-1. This example only has two factors because it is easier to visualize than a design with eight factors
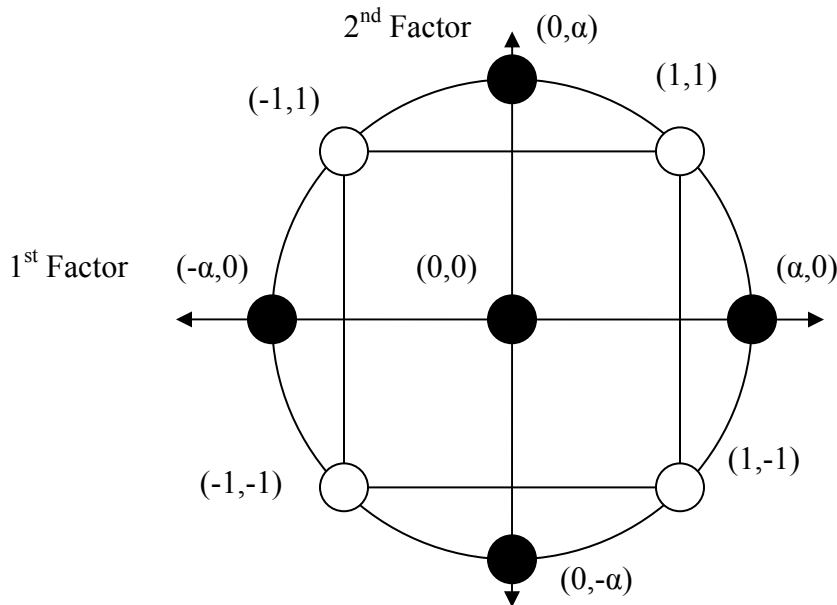
Figure 6-1: Graph of Central Composite Design

One advantage of the central composite design is the ability to detect higher order interactions. A two level factorial can only detect linear relationships while the additional star points give the ability to test for curvature in the model. The values for α are chosen so that the design will be rotatable. This means that the accuracy of the predictions made by the model are dependent solely on the distance from the centerpoint and not on the direction [8]. In the example shown in Figure 6-1 with two factors, any predictions made for points that lie on the circle would have the same accuracy. This will be important later on in the evaluation of the response surface. (Only in the case of two factors are the star points the came distance from the center as the corner points).

For the central composite design, the probe midpoint radius, r_{mid}, was increased to 2.8mm (.110in) to prevent further probe failure. The values for the four geometric features that were not selected for the composite design (X4, X7, X8 and X9) are in Table 6-1. The values for these parameters were chosen either as the midpoint from the screening experiment or as the value that matches the general design of existing CS4 tools.

Table 6-1: Constant Tool Parameters for the Central Composite Design

Parameter	Value	Parameter	Value
Step Spiral Starts, N_{ss}	2	Scroll Starts, N_{sc}	2
Scroll radius, r_{sc}	.64 mm (.025 in)	Scroll Land Fraction, L_a	.375

The geometric features that vary throughout the central composite design and their values are found in Table 6-2 and the tool configurations are found in Table 6-3.

Table 6-2: Factor Levels for Central Composite Design

	Probe Cone Angle	1/ Shoulder Radius	Shoulder Length	SS Pitch/ SS Starts	Scroll Pressure Angle
Factor Level	X1 $\varphi_p{}'$ deg	X2 $1/r_{sc}$ mm^{-1} (in^{-1})	X3 l_s mm (in)	X4 P_{ss}/N_{ss} mm (in)	X5 γ_p deg
-2	10	.008 (.2)	.8 (.03)	.5 (.020)	36
-1	17.5	.024 (.6)	1.5 (.06)	.6 (.025)	48
0	25	.039 (1)	2.3 (.09)	.8 (.030)	60
1	32.5	.055 (1.4)	3.0 (.12)	.9 (.035)	72
2	40	.071 (1.8)	3.8 (.15)	1.0 (.040)	84

Table 6-3: Central Composite Design

Tool	X1	X2	X3	X4	X5
1	-1	-1	-1	-1	1
2	1	-1	-1	-1	-1
3	-1	1	-1	-1	-1
4	1	1	-1	-1	1
5	-1	-1	1	-1	-1
6	1	-1	1	-1	1
7	-1	1	1	-1	1
8	1	1	1	-1	-1
9	-1	-1	-1	1	-1
10	1	-1	-1	1	1
11	-1	1	-1	1	1
12	1	1	-1	1	-1
13	-1	-1	1	1	1
14	1	-1	1	1	-1
15	-1	1	1	1	-1
16	1	1	1	1	1
17	-2	0	0	0	0
18	2	0	0	0	0
19	0	-2	0	0	0
20	0	2	0	0	0
21	0	0	-2	0	0
22	0	0	2	0	0
23	0	0	0	-2	0
24	0	0	0	2	0
25	0	0	0	0	-2
26	0	0	0	0	2
27	0	0	0	0	0

Figure 6-2: Tools for Central Composite Experiment

The weld parameters for the central composite design are almost the same as the screening experiment. Each of the 27 tools ran six welds at the same feed rates and plunge depth equation from the screening experiment. There was a slight modification to the spindle speeds so that the PHI varies linearly instead of using spindle speeds that varied linearly. The new spindle speeds are shown in Table 6-4. In total, 162 welds were run with the central composite tools. Each weld is at constant plunge depth and feed rate, but the spindle speed starts at the slowest spindle speed, reaches a steady state, increases to the intermediate spindle speed, achieves a steady state, and then increases to the fastest spindle speed.

Table 6-4: Spindle Speeds for Central Composite Design

Travel Speed	Spindle Speeds (RPM)		
mm/min (ipm)	Low	Medium	High
152 (6)	244	458	600
254 (10)	316	591	774

6.2 Central Composite Results

Similar to the screening experiment, the average forces, torques and temperatures for each weld were recorded to be used in the regression analysis. In addition to these response variables, the quality of each weld was determined using four different variables. These variables are the amount of flash, the size of any surface discontinuities, the surface roughness and the ledge distance.

6.2.1 Flash

In order to quantify the amount of flash, the welds were given a rating on a scale of zero to ten. A zero indicates that there is no flash, while a ten indicates that there is a large amount of flash. The scale was based on a set of welds that were selected from the welds that had been run for this central composite experiment. These welds were selected based on their varying amounts of flash. These welds are shown in Figure 6-3. The retreating side of the weld is shown at the bottom of each picture.
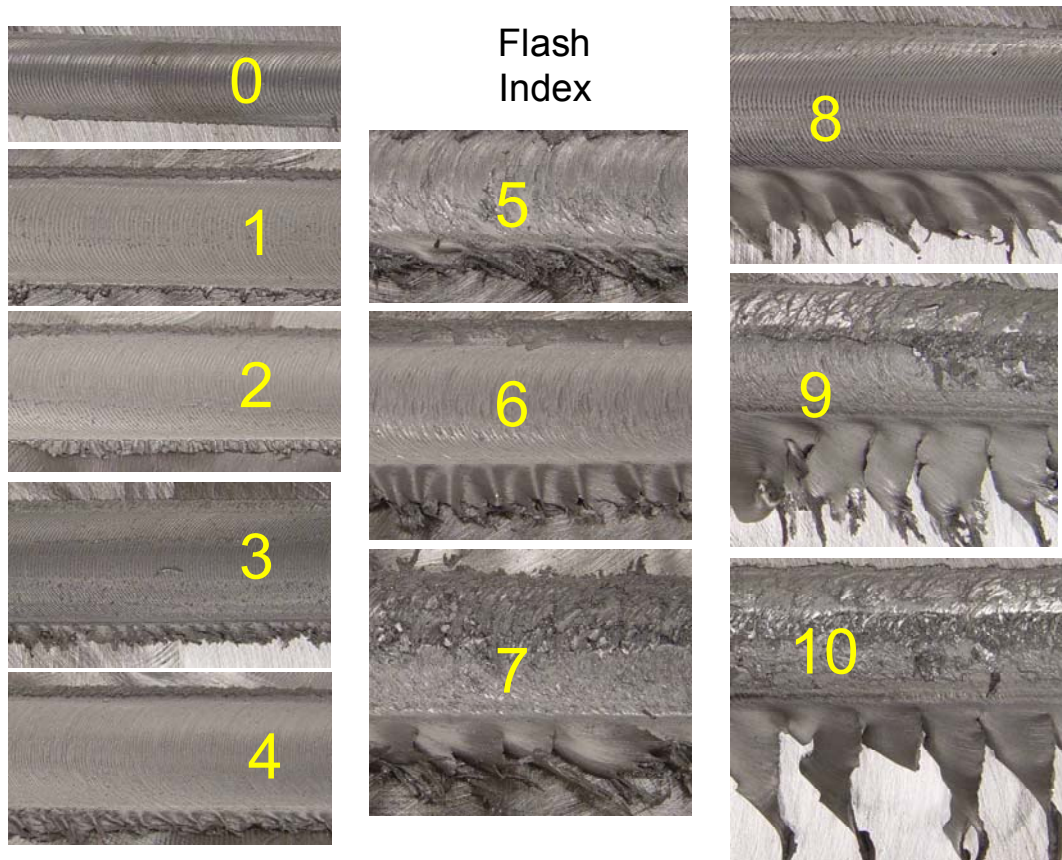
Figure 6-3: Flash Index

6.2.2   Surface Discontinuities

Some of the welds have weld discontinuity in the form of a trench that appears in the surface of the weld. For this study the associated response variable is the size of each discontinuity measured in millimeters across the surface of the weld. If there is no discontinuity, then the value for the response variable is zero. A typical discontinuity measurement is shown in Figure 6-4.
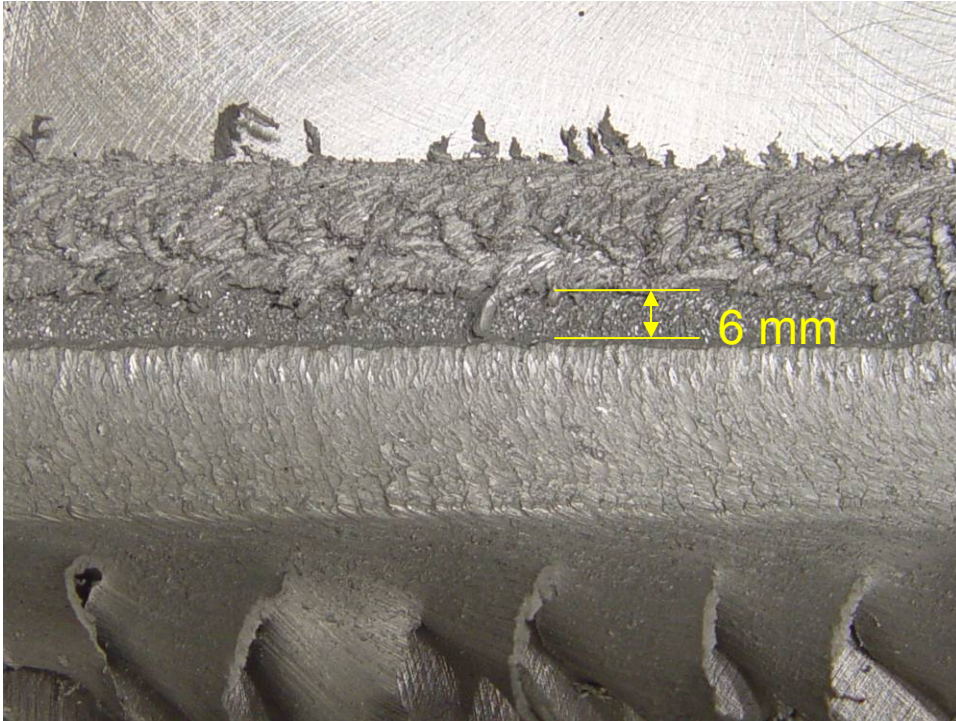
Figure 6-4: Surface Discontinuity Measurement

6.2.3 Surface Roughness

The surface roughness is measured in the same way that the flash is measured, by using a scale from zero to ten. A zero indicates that the surface is very smooth and a 10 indicates that the surface is very rough. Pictures showing examples of the scale are shown in Figure 6-5. There is not an apparent difference in the some of the lower valued welds shown, but the difference can be felt by touching the welds.

6.2.4 Ledge

The ledge is the distance from the advancing side edge to the deepest point in the weld. Some ledge measurements are shown in Figure 6-6.

Surface Roughness Index
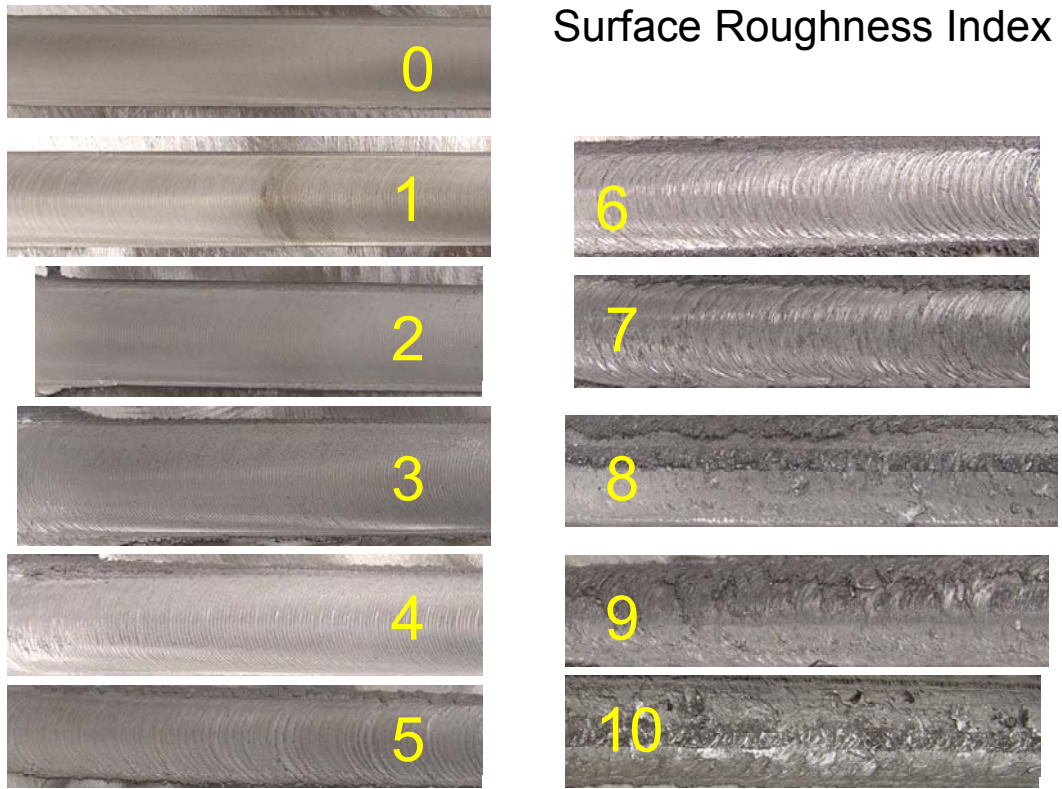
Figure 6-5: Surface Roughness Index
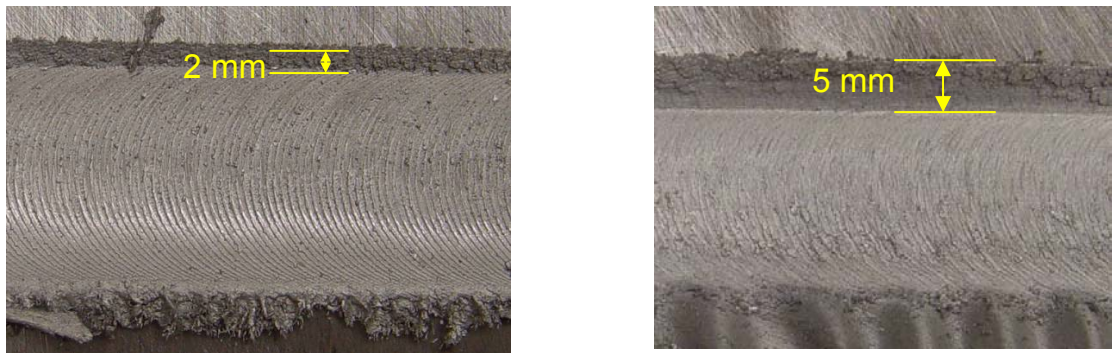
Figure 6-6: Ledge Measurements
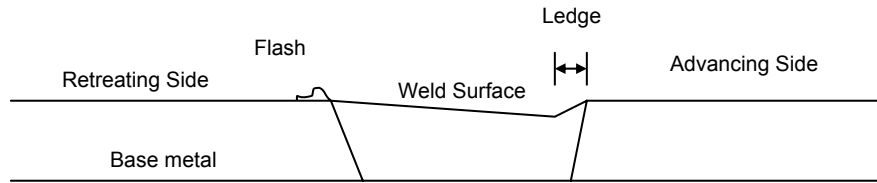
Figure 6-7: Cross-Section View of Ledge Measurement

6.2.5 Coefficient Matrix

Regressions were performed with the nine response variables being: longitudinal force (X), lateral force (Y), axial force (Z), tool temperature (Temp), spindle torque (Torque M), amount of flash (Flash), size of discontinuities (Discon), surface roughness (Rough) and ledge size (Ledge). The variables in the regression were the factor levels for each of the five geometric features (X1-X5) listed in Table 6-2; feed rate (X6), plunge depth (X7), and PHI (X8), all of the two-way and three-way interactions. Three-way interactions exclusively between geometric features are confounded with two-way interactions and are therefore not included in the regression

The purpose of the regression analysis was to determine a response surface based on the tool geometry and the weld parameters. To be extra sure that noise was not being modeled, the significance level was chosen to be a p-value of 0.01. Any factors or interactions that did not have a p-value less than 0.01 were dropped from the regression. Using the stepwise regression function in Minitab, all of the insignificant variables were eliminated from the nine regressions. The significant coefficients were put into a matrix form and are shown in Table 6-5. The units for the X, Y and Z forces are N; for the spindle torque , Nm; for the tool temperature, °C; and for the defect and ledge sizes, mm. The complete results of the regressions including residual plots are found in Appendix A.

Table 6-5: Coefficient Matrix

	X	Y	Z	Temp	Torque	Discon	Flash	Rough	Ledge
Constant	3769.4	-3160.9	30520.3	479.39	59.18	0.170	3.542	5.697	4.731
X1	0.0	480.1	1337.3	0.00	0.00	0.261	0.000	0.000	0.000
X2	297.2	0.0	2355.0	4.20	2.31	0.000	0.732	0.384	0.307
X3	936.5	-330.2	1533.6	7.63	0.00	0.000	0.854	0.310	0.522
X4	0.0	0.0	0.0	7.87	0.00	-0.086	0.000	0.000	0.000
X5	239.0	-572.8	-1025.0	0.00	0.99	0.299	0.498	0.310	0.312
X6	1412.1	-251.6	3370.4	0.00	-3.72	0.000	0.588	0.330	0.999
X7	1064.6	-482.6	6618.2	15.20	6.68	0.000	1.378	0.972	1.057
X8	1091.9	0.0	-499.7	30.82	-25.87	0.742	1.526	2.174	3.010
X1^2	0.0	-227.6	-433.7	3.18	0.00	0.195	0.151	0.123	0.000
X1X2	0.0	0.0	0.0	-5.03	0.00	0.000	0.000	0.000	0.000
X1X3	81.7	0.0	515.3	-9.96	0.00	0.000	0.000	0.000	0.000
X1X4	0.0	0.0	0.0	-5.51	0.00	0.000	0.000	0.000	0.000
X1X5	0.0	0.0	-438.4	-4.20	-0.80	0.149	0.000	0.173	0.381
X1X6	0.0	76.1	0.0	0.00	0.00	0.204	0.000	0.000	0.000
X1X8	-89.4	153.0	0.0	0.00	0.00	0.294	0.000	0.000	0.000
X2^2	0.0	-78.7	-608.8	0.00	-0.63	0.000	0.000	0.000	0.000
X2X3	0.0	0.0	-759.1	-4.14	-0.39	0.000	0.000	0.000	0.000
X2X4	0.0	0.0	0.0	3.84	0.00	0.000	0.150	0.132	0.000
X2X5	0.0	0.0	0.0	3.99	0.00	0.000	0.000	0.000	0.000
X2X6	0.0	0.0	0.0	-1.80	0.00	0.000	0.000	0.000	0.000
X2X7	146.8	0.0	0.0	-2.27	-0.41	-0.111	0.175	-0.187	0.000
X2X8	91.5	110.3	-576.5	-2.74	-2.22	-0.194	0.000	0.156	0.000
X3^2	0.0	0.0	-547.6	0.00	0.00	0.000	0.000	0.000	-0.178
X3X4	0.0	0.0	0.0	-3.02	0.00	0.000	0.000	0.000	0.000
X3X5	99.5	-191.9	0.0	2.91	0.00	0.219	0.230	0.180	0.000
X3X6	212.6	0.0	0.0	0.00	0.00	0.000	0.179	0.000	0.000
X3X7	344.9	-120.5	761.9	2.10	1.25	0.000	0.230	0.000	0.371
X3X8	202.9	90.2	0.0	0.00	0.00	0.201	0.000	0.000	0.000
X4^2	-73.1	135.8	0.0	-3.43	-0.63	-0.091	-0.154	0.000	-0.251
X4X5	0.0	0.0	-320.6	-7.19	0.00	0.000	0.000	0.000	0.214
X4X7	0.0	0.0	0.0	0.00	0.00	0.000	0.185	0.000	0.000
X4X8	-117.2	123.6	0.0	0.00	0.00	-0.104	0.000	-0.184	0.000
X5^2	0.0	158.3	306.2	-10.22	0.00	0.138	-0.272	-0.318	0.331
X5X6	183.6	-75.3	277.2	0.00	0.00	0.271	0.257	0.000	0.166
X5X7	120.2	-199.0	-352.4	0.00	0.00	0.222	0.199	0.000	0.000
X5X8	140.7	-261.1	0.0	0.00	0.00	0.583	0.380	0.323	0.342
X6X7	233.8	0.0	1034.7	0.00	0.00	0.000	0.193	0.000	0.000
X6X8	373.4	310.0	702.2	0.00	1.86	0.244	0.000	0.000	0.399
X7^2	143.0	0.0	0.0	0.00	0.00	0.000	0.000	0.000	0.000
X7X8	446.1	246.5	-513.2	-5.82	-4.46	0.262	0.223	0.376	0.506
X8^2	0.0	-165.8	-726.0	-15.62	14.39	0.327	0.000	-0.312	0.000
X1^2X6	0.0	0.0	0.0	0.00	-0.53	-0.017	0.000	0.000	0.000
X1^2X7	0.0	0.0	0.0	0.00	0.00	0.073	0.000	0.000	0.000
X1^2X8	0.0	0.0	0.0	0.00	0.00	0.052	0.000	0.000	0.000
X1X2X7	0.0	0.0	0.0	0.00	0.00	0.000	0.000	0.000	0.000
X1X5X7	0.0	0.0	0.0	0.00	0.00	0.000	0.179	0.000	0.000
X1X5X8	0.0	0.0	0.0	0.00	0.00	0.167	0.000	0.000	0.247
X1X6X7	0.0	0.0	0.0	0.00	0.00	0.106	0.000	0.000	0.000
X1X6X8	0.0	0.0	0.0	0.00	0.00	0.167	0.000	0.000	0.000
X2^2X7	0.0	0.0	-325.3	0.00	0.00	0.000	0.000	0.000	0.000
X2X4X7	0.0	0.0	0.0	0.00	0.00	0.000	0.200	0.000	0.000
X2X5X8	0.0	-130.2	-392.9	0.00	0.00	0.000	0.000	0.000	0.000
X2X6X7	0.0	0.0	0.0	0.00	0.00	0.000	0.000	0.000	-0.199
X2X6X8	-98.2	0.0	0.0	0.00	0.00	0.000	0.000	0.000	0.000
X2X7^2	0.0	0.0	0.0	0.00	0.00	-0.208	0.000	0.000	0.000
X2X8^2	-169.2	0.0	0.0	0.00	1.43	0.000	0.000	0.000	0.000
X3^2X6	0.0	0.0	-266.4	0.00	-0.30	0.000	0.000	0.000	0.000
X3^2X7	0.0	97.4	-400.5	0.00	-0.56	0.000	-0.164	0.000	0.000
X3^2X8	0.0	0.0	0.0	0.00	0.00	0.000	0.000	0.000	-0.252
X3X5X6	0.0	0.0	-313.5	-1.85	-0.40	0.000	0.000	0.000	0.000
X3X5X7	0.0	0.0	0.0	0.00	0.00	0.000	0.000	-0.197	0.000
X3X5X8	0.0	-110.5	0.0	0.00	0.00	0.240	0.000	0.000	0.000
X3X6X8	0.0	124.8	0.0	0.00	0.00	0.000	0.000	0.000	0.000
X3X7^2	0.0	0.0	0.0	0.00	0.99	0.000	0.000	0.000	0.000
X3X7X8	0.0	191.7	0.0	0.00	-0.69	0.000	0.000	0.000	0.000
X3X8^2	-146.4	0.0	-632.6	0.00	0.00	0.201	0.000	0.000	0.000
X4^2X8	0.0	0.0	0.0	0.00	0.00	0.000	0.000	0.000	0.000
X4X5X7	0.0	0.0	0.0	0.00	0.00	0.000	0.231	0.000	0.000
X4X6X7	0.0	0.0	0.0	0.00	0.37	0.000	0.151	0.000	0.218
X4X8^2	-107.5	157.7	0.0	0.00	0.00	-0.156	0.000	0.000	0.000
X5^2X6	0.0	0.0	0.0	0.00	0.00	0.179	0.000	0.000	0.000
X5^2X7	0.0	0.0	0.0	1.82	0.00	0.160	0.000	0.000	0.000
X5^2X8	0.0	0.0	490.5	0.00	0.00	0.115	0.000	-0.134	-0.262
X5X6X7	0.0	0.0	0.0	0.00	0.46	0.000	0.151	0.000	0.000
X5X6X8	0.0	0.0	0.0	0.00	0.00	0.278	0.000	0.000	0.000
X5X7X8	0.0	0.0	0.0	0.00	0.00	0.208	0.000	0.000	0.000
X5X8^2	0.0	267.4	1018.9	0.00	0.00	0.285	0.000	0.000	0.000
X6X7X8	-231.4	111.9	-750.9	0.00	0.00	0.000	-0.246	0.000	0.000
X6X8^2	-336.4	0.0	0.0	0.00	2.22	0.000	0.000	0.000	-0.370
X7X8^2	-289.1	0.0	0.0	0.00	2.90	0.000	0.000	-0.354	0.000

53

The residual plots of each of the nine regressions show that there are no obvious trends when comparing the residuals to the observation order or to their fitted value. The only exception to this are the residuals from the Tool Temperature regression plotted against the observation order. Some possible explanations are that the anvil that supported the workpiece heated up more with consecutive runs, that different thermocouples did not work the same or that the cooling mechanism in the tool holder worked differently at different times. Since none of these explanations were quantified at the time of the experimentation, it is not possible to use them as variables in the regression.

The normal probability plots and the histograms also show that the residuals are normally distributed. There are a few outliers that show up in some of the measurements of the response surfaces, but they aren't of great concern given that the some of the scales were subjective and that some significant variables from the screening experiment were not tested. Considering that FSW is a pretty noisy process, the fits are very good.

6.3   Composite Design Discussion of Results

With the coefficients all determined, it is now possible to predict all of the response variables based on the tool geometry and the weld parameters. Of course one of the limitations is that the geometric features must be within the factor level range (-1, 1). An estimate may be made outside of these bounds but the uncertainty increases drastically outside of these limits. Within these bounds an estimate of the error of a prediction can be calculated by using the S value found in the regression analysis. For an

approximate 95% confidence interval, twice the S value should be added to the prediction for an upper bound and subtracted from the prediction for a lower bound.

With the response surface equations, it is possible to calculate a value that doesn't really make sense. For example, a negative value for the amount of flash can be achieved with the right combination of parameters. Obviously, there can't be negative flash. This prediction should be treated as a zero flash prediction. It may be beneficial to find these values because the more negative they are, the less likely the weld is to have any flash. The same is true for the size of discontinuity, the surface roughness and the ledge size. Most of the welds did not have a discontinuity. Therefore the real value of the discontinuity size equation is to predict which welds are likely to have a discontinuity and not to compare welds that don't have any discontinuities at all.

Because of the complexity of the equations, the next step in using these response surfaces is to use optimization software to determine the best welds possible. However, this step requires a clear objective. Some applications may require that the weld have as little flash as possible with the lowest axial force. Other applications may desire a minimal longitudinal force without regard to the other response variables. Almost all applications will require zero discontinuities. The individual user must determine what minimum weld quality is sufficient and then try to optimize the process based on the particular desired output.

It is difficult to look at the matrix of coefficients and see what the effect varying each of the features of tool geometry will have on the response surface. To try and illustrate the effect of tool geometry, some examples of response surfaces are provided. Some sample ranges of the response surfaces for constant process parameters are given as

well as minimum and maximum values of different response surfaces for unconstrained situations and also for a situation in which there are constraints on the weld quality.

6.3.1 Response Variable Ranges

In order to show a small sample of the variation provided by the geometric features, the response surface equations were used to determine the responses for a particular set of process parameters. Leaving the process parameters at the centerpoint values (factor level equal to zero), all combinations of the high and low values (-1, 1) for the five geometric features were used to calculate each of the response surfaces. Since there were five variables and two levels for each variable, there were 2^5 combinations to calculate. The maximum and minimum values for each of these 32 combinations are shown in Table 6-6.

Table 6-6: Predicted Response Variable Ranges for Particular Set of Process Parameters

	X1	X2	X3	X4	X5	Minimum	Maximum
Longitudinal	1	-1	-1	-1	-1	2240 N	
Force (X)	1	1	1	-1	1		5350 N
Lateral Force	1	-1	-1	-1	-1	-1980 N	
(Y)	-1	1	1	-1	1		-4750 N
Axial Force (Z)	-1	-1	-1	1	1	22860 N	
	1	1	1	1	-1		36000 N
Tool	-1	-1	-1	-1	-1	421 °C	
Temperature	-1	1	1	1	1		510 °C
Spindle Torque	-1	-1	-1	-1	-1	53 Nm	
	-1	1	-1	-1	1		62 Nm
Surface	-1	-1	1	1	-1	-.3 mm	
Discontinuities	1	-1	1	-1	1		1.4 mm
Amount of	-1	-1	-1	1	-1	1.3	
Flash	-1	1	1	1	1		5.7
Surface	1	-1	-1	1	-1	4.4	
Roughness	1	1	1	1	1		7.0
Ledge Size	1	-1	-1	1	-1	2.9 mm	
	1	1	1	1	1		6.4 mm

As shown in Table 6-6, tool geometry alone can more than double the longitudinal and lateral forces, the amount of flash and the ledge size. It can also increase the axial force by more than 50% and substantially increase the likeliness of a weld defect. For different combinations of process parameters, the impact might be even greater than the example shown in Table 6-6.

6.3.2   Unconstrained Response Minimums and Maximums

To show how the variables change at different points on the response surface, the maximum and minimum points of each of the response surface were calculated. By comparing the factor levels of each of the variables for the minimum and maximum response values, the effect of each of the geometric features becomes more evident. In this section the only constraint on the optimization is how far the factor levels are allowed to change. There are two options and each has an advantage. The first option is to let the variables extend out to the surface of the circle as shown in Figure 6-1. This allows for the greatest number of possibilities. The disadvantage is that if one of the factors is dominant, it will have a large magnitude and the other variables will reduce to zero and their effect on the response surface wll not be apparent. The other option is to constrain the varaible factor levels to be within the square shown in Figure 6-1. This option has less possibilities so the global minimum might not be within the optimization. The advantage is that as one variable increases or decreases, its value does not directly constrain any of the other variables. Both of these options were used. (In the case of the 8 factors that were used for the response surface, a circle and sqaure are not really the constraining features; but since there is no term for an 8-dimensional circle or square, these terms will be used.)

Another problem in calculating minima and maxima for a response surface is that there are often local minima and maxima to which optimization software will converge instead of converging to a global minima and maxima. In an attempt to find a global minimum and maximum for the response surfaces, different starting points were used for the optimization process using the fmincon function from Matlab. 16 different starting points were used and they are shown in Table 6-7.

Table 6-7: Start Points for Optimization

Start	X1	X2	X3	X4	X5	X6	X7	X8
1	-1	-1	-1	-1	-1	-1	-1	-1
2	1	-1	-1	-1	1	-1	1	1
3	-1	1	-1	-1	1	1	-1	1
4	1	1	-1	-1	-1	1	1	-1
5	-1	-1	1	-1	1	1	1	-1
6	1	-1	1	-1	-1	1	-1	1
7	-1	1	1	-1	-1	-1	1	1
8	1	1	1	-1	1	-1	-1	-1
9	-1	-1	-1	1	-1	1	1	1
10	1	-1	-1	1	1	1	-1	-1
11	-1	1	-1	1	1	-1	1	-1
12	1	1	-1	1	-1	-1	-1	1
13	-1	-1	1	1	1	-1	-1	1
14	1	-1	1	1	-1	-1	1	-1
15	-1	1	1	1	-1	1	-1	-1
16	1	1	1	1	1	1	1	1

For some of the response surfaces, several local minima or maxima were found. While for some response surfaces, the optimization converges to a single global minimum or maximum. The complete tables containing all of the converged values for each of the response surfaces is found in Appendix B. The number of times to which a praticular solution was converged are also shown. There are a total of 32 diffent minima and 32 maxima. 16 for the convergence within the circle and 16 for the convergence within the square. Table 6-8 and Table 6-9 show the minimum and maximum values that

the optimization found to demonstrate the information that can be learned from looking at the different maximum and minimum values.

Table 6-8: Minimum Longitudinal Force (X)

X1	X2	X3	X4	X5	X6	X7	X8	Minimum	#
0.61	-0.64	-1.89	0.22	0.77	-1.00	-1.00	0.22	520	4
0.24	-0.23	-2.16	-0.04	0.49	-1.00	1.00	-1.00	300	12
1.00	-1.00	-1.00	-1.00	1.00	-1.00	-1.00	0.09	810	2
1.00	-1.00	-1.00	1.00	1.00	-1.00	-1.00	0.25	770	8
-1.00	-1.00	-1.00	-1.00	1.00	-1.00	1.00	-1.00	1020	2
-1.00	-1.00	-1.00	1.00	1.00	-1.00	1.00	-1.00	1040	4

Table 6-9: Maximum Longitudinal Force (X)

X1	X2	X3	X4	X5	X6	X7	X8	Maximum	#
0.08	0.31	1.95	-0.22	1.03	1.00	1.00	1.00	11730	16
-1.00	1.00	1.00	-1.00	1.00	1.00	1.00	1.00	10440	16

The first step in analyzing the results of the optimization is to look for large magnitudes in the circle-constrained results. X3 has the largest magnitude for both the minimum and maximum and is at a positive value for the maximum and at a negative value for the minimum. Therefore, as X3 increases, so does the longitudinal force. The values of X3 in the square-constrained optimization confirm this hypothesis as does the positive coefficient for X3 that can be found in Table 6-5.

The only other factor that exceeds a magnitude of one is X5. The levels for X5 are positive in both the local minima and the local maxima. A check of the coefficients in Table 6-5 shows that X5 has large coefficients for its interactions with each of the process parameters.

After the factors with large magnitudes have been evaluated, another step is to check for any other variables that are consistently negative for the minima and positive for the maxima or vice versa. X2 fits this description. Therefore, as X2 increases, so does the longitudinal force. However, X2 does not have as large of an effect as X3, which is confirmed by inspection of the values of the coefficients. The other two geometric factors, X1 and X4, do not have any immediately recognizable patterns.

The same type of analysis was done for each of the response surfaces and the results are compiled in Table 6-10. A plus sign indicates that as this factor level increases, so does the response variable. A minus sign indicates that as this factor level increases, the response variable decreases. INT indicates that the interaction effects were dominant. The factors that had the largest magnitudes have an asterisk. If the relative size of the effects of the process parameters is larger than the geometric parameters, they are also shown . For example, in the case of the torque, the PHI had coefficients that were almost 10 times larger than the coefficients for the geometric features

Table 6-10: Summary of Response Surface Effects

Name	Probe Cone Angle	1/ Shoulder Radius	Shoulder Length	SS Pitch/ SS Starts	Scroll Pressure Angle	Feed Rate	Plunge Depth	PHI
Factor	X1	X2	X3	X4	X5	X6	X7	X8
Longitudinal Force (X)		+	+*		INT			
Lateral Force (Y)	-*				INT*			
Axial Force (Z)	+	+*	+		INT*	1.5	3	
Tool Temperature	INT*				INT*		2	4
Spindle Torque		+*	+*		+		2	10
Discontinuity Size				-*	INT*			2
Flash		+	+		INT*		1.5	1.5
Surface Roughness		+			INT*		3	6
Ledge Size		+	+	INT*	INT		2	6

The trends that are shown in Table 6-10 may not always hold true. There may be certain constraints and interactions that override these general trends for a particular application, but they are still useful in giving approximations of the effect that each of the variables has on the each of the response surfaces.

6.3.3   Constrained Response Minimum and Maximum

The examples that were addressed previously did not consider that it might be advantageous to minimize certain responses while maintaining a constraint on other responses. An example of this might be trying to minimize the power input (spindle torque multiplied by spindle speed), while maintaining a high feed rate, low amount of flash, minimizing the chance of a defect, having a good surface finish and a small ledge size.

Table 6-11 shows the results of minimizing the power input and constraining the defect size to be less than 0 mm, the amount of flash to be less than 0, the surface roughness to be less than 2.5 and the ledge size to be less than 0.5 mm. The same 16 start points from Table 6-7 were used for this optimization routine.

Table 6-11: Minimized Axial Force with Constraints

Geometric Features					Process Parameters		
X1	X2	X3	X4	X5	X6	X7	X8
-0.04	-2.23	0.01	0.13	-0.14	1.00	-1.00	-1.00
Response Variables							
X	Y	Z	Temp	Torque	Disc	Flash	Rough	Ledge
2730 N	-3170 N	16100 N	396 °C	64.6 Nm	-0.5 mm	-0.3	2.4	0.2 mm

Table 6-11 shows that the optimization routine converged to the same minimum for all 16 start points.

7 Conclusion

Perhaps the most important conclusion that can be drawn from this study is that the geometry of a particular tool can make a large difference in several different responses variables. The pilot study showed that there is a noticeable difference in the performance of different tool geometries and that all of the different variations of the geometric features would be able to make consolidated welds within the process window. With this confidence, a screening experiment was designed to compare the impact of each of these features against each other.

The screening experiment went on to show that all of the nine geometric features chosen to be studied in this thesis were statistically significant in determining the process forces, torque and tool temperature. However, the probe cone angle, the shoulder radius of curvature, the shoulder length and the scroll pressure angle all had much larger coefficients in the regression analyses that were performed. This indicated that their relative significance was greater than the rest of the geometric features. With this separation of the variables, a central composite design was chosen that would provide a response surface to quantify the effect of each of these variables. Since a central composite design could be expanded to include five variables instead of just the four already mentioned, by adding only two tools, the step spiral pitch divided by the number

of step spiral starts was also selected because of its possible significance in affecting the surface finish.

The central composite design gave exact coefficients for a complicated response surface for each of the response variables: longitudinal force (X), lateral force (Y), axial force (Z), tool temperature, spindle torque, defect size, amount of flash, surface roughness and ledge size. Using the coefficients from the regression analyses, optimization routines were run to establish minimum and maximum points for each of the response surfaces. These minima and maxima show the trends that exist within the selected window of the factor levels of the variables. Some of the trends are not easily distinguishable because of the complicated interactions, but most of the significant trends can be identified.

7.1   How Each of the Response Variables are Affected by Geometry

- Longitudinal Force (X): Increases as shoulder length increases and shoulder radius decreases; also affected by interactions between scroll pressure angle and process parameters.

- Lateral Force (Y): Increases as probe cone angle decreases; also affected by interactions between scroll pressure angle and process parameters.

- Axial force (Z): Increases as shoulder radius decreases and as probe cone angle and shoulder length decrease; also affected by interactions between scroll pressure angle and process parameters.

- Tool Temperature: Affected by interactions between scroll pressure angle, probe cone angle and process parameters.

- Spindle Torque: Increases as shoulder radius decreases and as shoulder length and scroll pressure angle increase.

- Discontinuity Size: Increases as step spiral pitch decreases; also affected by interactions between scroll pressure angle and process parameters.

- Amount of Flash: Increases as shoulder radius decreases and as shoulder length decreases; also affected by interactions between scroll pressure angle and process parameters.

- Surface Roughness: Increases as shoulder radius decreases; also affected by interactions between scroll pressure angle and process parameters.

- Ledge Size: Increases as shoulder radius decreases and as probe cone angle and shoulder length decrease; also affected by interactions between scroll pressure angle, step spiral pitch and process parameters.

7.2 Effects of Each Geometric Feature

- Probe Cone Angle: A larger cone angle decreases the lateral force and increases the axial force. It is also involved in interaction effects that change the tool temperature.

- Shoulder Radius: A flatter shoulder decreases the longitudinal force and axial forces, the spindle torque, the amount of flash, the surface roughness and the ledge size.

- Shoulder Length: A larger shoulder length increases the longitudinal force and axial forces, the spindle torque, the amount of flash and the ledge size.

- Step Spiral Pitch: A larger step size on the step spiral decreases the chances of having a surface discontinuity and also interacts with process parameters to affect the ledge size

- Scroll Pressure Angle: Interacts with process parameters to affects all of the response surfaces

7.3   Possible Physical Explanations

In this section a brief look at some of the possible physical explanations for the way that the response surfaces are affected by the tool geometry is provided.

The scroll pressure angle interacting with the process parameters would affect the flow patterns that the workpiece material would follow. It would also have a large effect on the frictional heating of the workpiece. These would in turn affect the process forces, temperature and the surface quality of the weld.

The shoulder radius and the shoulder length affect nearly the same set of response surfaces. They are probably related because they both affect the cross-sectional area and the total volume of the tool that is plunged into the material. The change in cross-section and volume would be significant in the forces required to move material to the other side of the tool and also in determining the location where the displaced material ends up.

The step spiral on the probe and the probe cone angle affect the flow around the probe and the vortex flow, which in turn affect several of the response surfaces.

8 Future Work

One of the next steps in understanding the full effects of this study is to try the same type of experimentation on a workpiece of a different material. The response surfaces developed in this study are specific to welds in Aluminum 7075 T-651. It is logical to assume that other aluminum alloys might have similar responses to changes in tool geometry. Without further study, it is difficult to extrapolate what the effects would be in other materials.

The CS4 tool is only one small piece of the possible different tool configurations. There are endless possibilities that can be explored. For example, the scroll on the shoulder is assumed to be a circular arc, but an ellipse or parabola shaped scroll might work even better. Another possibility that deserves exploration and also may influence tool geometry is tool material. Different tool materials may experience more or less shear forces on the workpiece and thereby alter the necessary size of the scroll or the step spiral.

As the flow characteristics and heat transfer of friction stir processing are better understood, more specific explanations may be possible for the reasons that certain geometric features impact specific responses more than other geometric features. But for now, using response surface methodology is the best predictor of the effect of tool geometry on the friction stir process.

9 References

1. Aliabadi, M. H., 1999, "Residual-Stress-Field-Effects," http://www3.inperial.ac.uk/aeronautics/wingcentre/aerostructures/aerostructure/residualstressfield/

2. Cederqvist, L., "Evaluation and Analysis of Lid #61: weld KL235-246", SKB Report, Sept. 2007.

3. Zettler, R. et al., "A Study on Material Flow in FSW of AA 2024-T351 and AA 6056-T4 Alloys", 5th International Symposium on Friction Stir Welding, Metz, France, 14-16 Sept. 2004.

4. Colegrove, P.A., H.R. Shercliff and T. Hyoe, "Development of the Trivex™ Friction Stir Welding Tool for Making Lap Welds", 5th International Symposium on Friction Stir Welding, Metz, France, 14-16 Sept. 2004.

5. Pew, J.W., T.W. Nelson and C.D. Sorensen, "Torque based weld power model of friction stir welding", *Science and Technology of Welding and Joining*, 12:4 (July 2007), pp. 341-347.

6. Lawson, J. and J. Erjavec. *Modern Statistics for Engineering and Quality Improvement*. Pacific Grove, CA: Duxbury, 2001.

7. S.K. Chimbli. et al., "Minimizing lack of consolidation defects in friction stir welds", Friction Stir Welding and Processing IV, TMS (The Minerals, Metals & Materials Society), 2007.

8. Myers, R. H. *Response Surface Methodology*. 1976.

Appendix A.   Central Composite Regressions

```
The regression equation is
X = 847 + 66.8 X2 + 211 X3 + 53.7 X5 + 317 X6 + 239 X7 + 245 X8 + 18.4 X1X3
    - 20.1 X1X8 + 33.0 X2X7 + 20.6 X2X8 + 22.4 X3X5 + 47.8 X3X6 + 77.5 X3X7
    + 45.6 X3X8 - 16.4 X4^2 - 26.4 X4X8 + 41.3 X5X6 + 27.0 X5X7 + 31.6 X5X8
    + 52.6 X6X7 + 83.9 X6X8 + 32.2 X7^2 + 100 X7X8 - 22.1 X2X6X8 - 38.0 X2X8^2
    - 32.9 X3X8^2 - 24.2 X4X8^2 - 52.0 X6X7X8 - 75.6 X6X8^2 - 65.0 X7X8^2


Predictor      Coef  SE Coef       T        P
Constant     847.43    10.80   78.50    0.000
X2            66.82    10.04    6.65    0.000
X3           210.55    10.04   20.97    0.000
X5           53.727    5.797    9.27    0.000
X6          317.465    9.557   33.22    0.000
X7           239.34    11.46   20.89    0.000
X8          245.482    6.776   36.23    0.000
X1X3         18.372    7.100    2.59    0.010
X1X8        -20.098    7.484   -2.69    0.008
X2X7         32.995    7.100    4.65    0.000
X2X8         20.579    7.099    2.90    0.004
X3X5         22.376    7.100    3.15    0.002
X3X6         47.805    5.797    8.25    0.000
X3X7         77.533    7.100   10.92    0.000
X3X8         45.617    7.099    6.43    0.000
X4^2        -16.441    5.546   -2.96    0.003
X4X8        -26.353    7.099   -3.71    0.000
X5X6         41.271    5.797    7.12    0.000
X5X7         27.023    7.100    3.81    0.000
X5X8         31.635    7.099    4.46    0.000
X6X7         52.557    6.769    7.76    0.000
X6X8         83.946    6.767   12.40    0.000
X7^2          32.15    11.71    2.75    0.006
X7X8        100.298    8.295   12.09    0.000
X2X6X8      -22.083    7.099   -3.11    0.002
X2X8^2       -38.04    12.30   -3.09    0.002
X3X8^2       -32.91    12.30   -2.68    0.008
X4X8^2      -24.171    7.100   -3.40    0.001
X6X7X8      -52.016    8.298   -6.27    0.000
X6X8^2       -75.63    11.71   -6.46    0.000
X7X8^2       -64.99    14.23   -4.57    0.000


S = 120.476   R-Sq = 93.6%   R-Sq(adj) = 93.2%
```

```
Analysis of Variance

Source          DF        SS        MS        F       P
Regression       30  94681742   3156058  217.44   0.000
Residual Error  445   6458940     14514
Total           475 101140682
```

Residual Plots for X

Normal Probability Plot

Versus Fits

Histogram

Versus Order
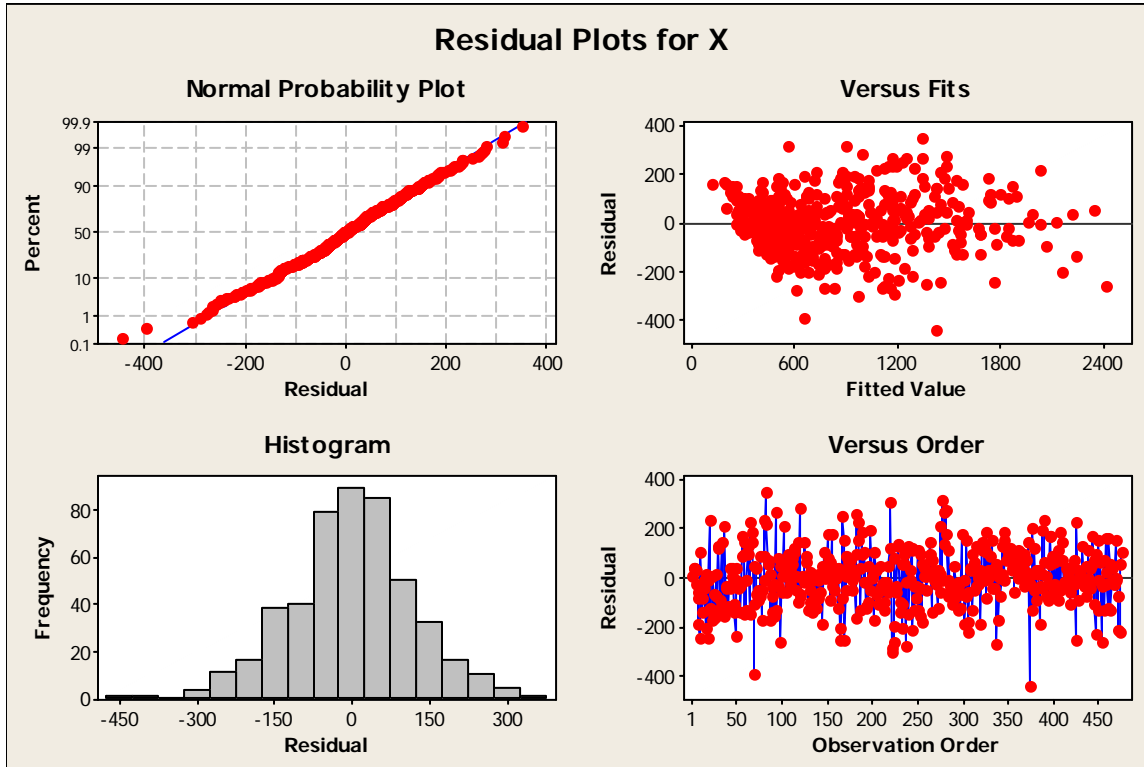
Figure A-1: Residual Plots for Longitudinal Force (X)

```
The regression equation is
Y = - 711 + 108 X1 - 74.2 X3 - 129 X5 - 56.6 X6 - 108 X7 - 51.2 X1^2 + 17.1 X1X6
    + 34.4 X1X8 - 17.7 X2^2 + 24.8 X2X8 - 43.1 X3X5 - 27.1 X3X7 + 20.3 X3X8
    + 30.5 X4^2 + 27.8 X4X8 + 35.6 X5^2 - 16.9 X5X6 - 44.7 X5X7 - 58.7 X5X8
    + 69.7 X6X8 + 55.4 X7X8 - 37.3 X8^2 - 29.3 X2X5X8 + 21.9 X3^2X7
    - 24.8 X3X5X8 + 28.1 X3X6X8 + 43.1 X3X7X8 + 35.5 X4X8^2 + 60.1 X5X8^2
    + 25.2 X6X7X8
```

Predictor	Coef	SE Coef	T	P
Constant	-710.64	19.10	-37.21	0.000
X1	107.941	6.505	16.59	0.000
X3	-74.240	6.096	-12.18	0.000
X5	-128.77	10.56	-12.19	0.000
X6	-56.558	5.818	-9.72	0.000
X7	-108.495	9.485	-11.44	0.000
X1^2	-51.179	7.062	-7.25	0.000
X1X6	17.111	6.416	2.67	0.008
X1X8	34.400	7.865	4.37	0.000
X2^2	-17.699	6.491	-2.73	0.007
X2X8	24.791	7.466	3.32	0.001
X3X5	-43.149	7.467	-5.78	0.000
X3X7	-27.091	7.467	-3.63	0.000
X3X8	20.282	7.466	2.72	0.007
X4^2	30.528	6.491	4.70	0.000
X4X8	27.795	7.466	3.72	0.000
X5^2	35.582	6.491	5.48	0.000
X5X6	-16.940	6.096	-2.78	0.006
X5X7	-44.740	7.467	-5.99	0.000
X5X8	-58.705	7.466	-7.86	0.000
X6X8	69.691	7.118	9.79	0.000
X7X8	55.418	8.725	6.35	0.000
X8^2	-37.28	12.31	-3.03	0.003
X2X5X8	-29.266	9.144	-3.20	0.001
X3^2X7	21.899	7.130	3.07	0.002
X3X5X8	-24.838	9.144	-2.72	0.007
X3X6X8	28.065	7.466	3.76	0.000
X3X7X8	43.089	9.144	4.71	0.000
X4X8^2	35.457	7.466	4.75	0.000
X5X8^2	60.12	12.93	4.65	0.000
X6X7X8	25.156	8.727	2.88	0.004

```
S = 126.705   R-Sq = 76.4%   R-Sq(adj) = 74.8%
```

Analysis of Variance

Source	DF	SS	MS	F	P
Regression	30	23122885	770763	48.01	0.000
Residual Error	445	7144155	16054		
Total	475	30267040			
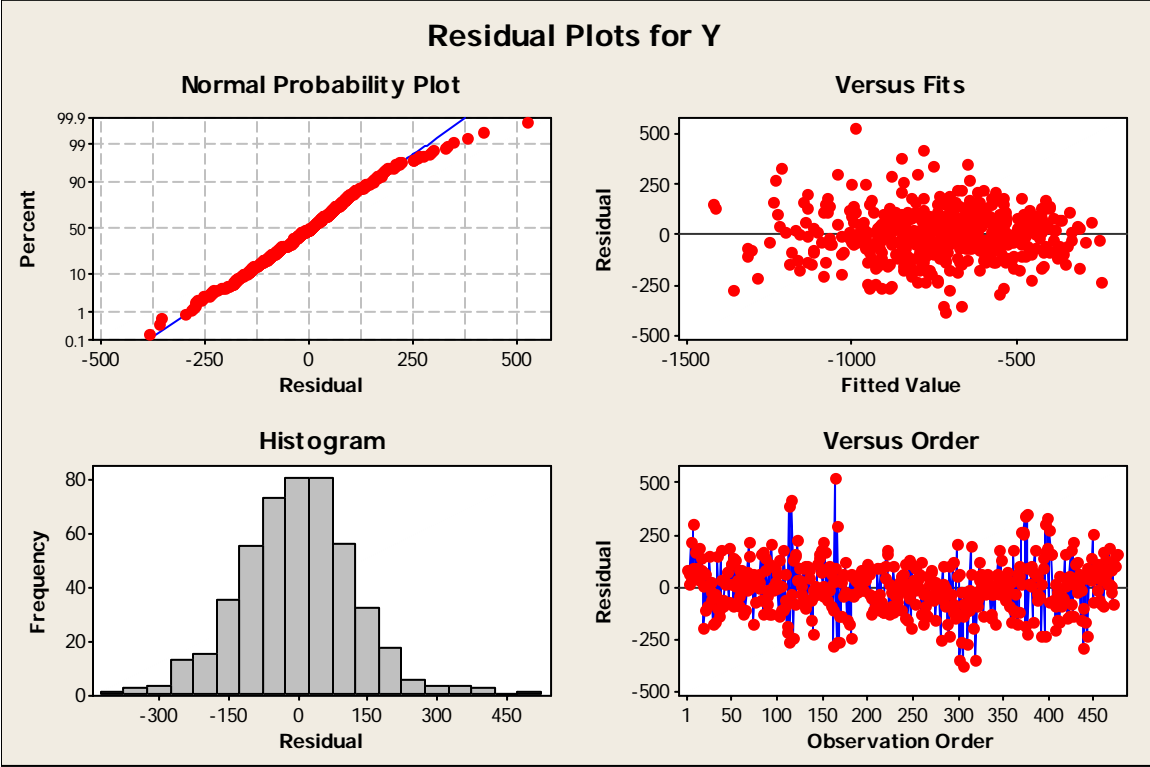
Figure A-2: Residual Plots for Lateral Force (Y)

```
The regression equation is
Z = 6862 + 301 X1 + 529 X2 + 345 X3 - 230 X5 + 758 X6 + 1488 X7 - 112 X8
    - 97.5 X1^2 + 116 X1X3 - 98.6 X1X5 - 137 X2^2 - 171 X2X3 - 130 X2X8
    - 123 X3^2 + 171 X3X7 - 72.1 X4X5 + 68.8 X5^2 + 62.3 X5X6 - 79.2 X5X7
    + 233 X6X7 + 158 X6X8 - 115 X7X8 - 163 X8^2 - 73.1 X2^2X7 - 88.3 X2X5X8
    - 59.9 X3^2X6 - 90.0 X3^2X7 - 70.5 X3X5X6 - 142 X3X8^2 + 110 X5^2X8
    + 229 X5X8^2 - 169 X6X7X8


Predictor      Coef    SE Coef        T       P
Constant    6861.58      67.10   102.27   0.000
X1           300.65      22.86    13.15   0.000
X2           529.46      21.42    24.72   0.000
X3           344.79      37.10     9.29   0.000
X5          -230.45      37.10    -6.21   0.000
X6           757.74      27.64    27.41   0.000
X7          1487.91      43.47    34.23   0.000
X8          -112.34      33.86    -3.32   0.001
X1^2         -97.51      24.82    -3.93   0.000
X1X3         115.86      26.24     4.42   0.000
X1X5         -98.56      26.24    -3.76   0.000
X2^2        -136.87      22.81    -6.00   0.000
X2X3        -170.67      26.24    -6.51   0.000
X2X8        -129.60      26.23    -4.94   0.000
X3^2        -123.11      22.81    -5.40   0.000
X3X7         171.30      26.24     6.53   0.000
X4X5         -72.07      26.24    -2.75   0.006
X5^2          68.83      22.81     3.02   0.003
X5X6          62.31      21.42     2.91   0.004
X5X7         -79.22      26.24    -3.02   0.003
X6X7         232.62      25.06     9.28   0.000
X6X8         157.86      25.01     6.31   0.000
X7X8        -115.37      30.65    -3.76   0.000
X8^2        -163.23      43.26    -3.77   0.000
X2^2X7       -73.13      25.66    -2.85   0.005
X2X5X8       -88.33      32.13    -2.75   0.006
X3^2X6       -59.89      20.50    -2.92   0.004
X3^2X7       -90.04      25.66    -3.51   0.000
X3X5X6       -70.48      26.24    -2.69   0.007
X3X8^2      -142.21      45.43    -3.13   0.002
X5^2X8       110.28      25.11     4.39   0.000
X5X8^2       229.07      45.43     5.04   0.000
X6X7X8      -168.82      30.66    -5.51   0.000


S = 445.169   R-Sq = 92.6%   R-Sq(adj) = 92.1%


Analysis of Variance

Source           DF          SS         MS       F       P
Regression       32  1101004930   34406404  173.62   0.000
Residual Error  443    87791833     198176
Total           475  1188796763
```
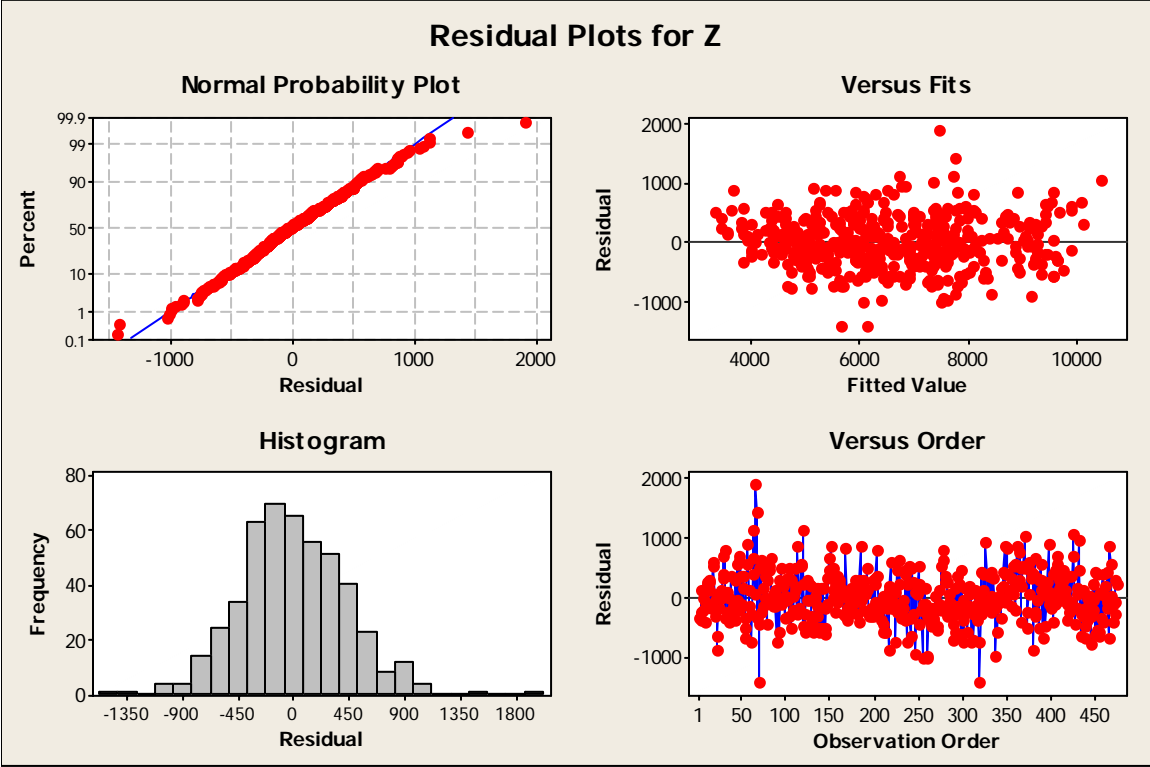
Figure A-3: Residual Plots for Axial Force (Z)

```
The regression equation is
Temp = 479 + 4.20 X2 + 7.63 X3 + 7.87 X4 + 15.2 X7 + 30.8 X8 + 3.18 X1^2
        - 5.03 X1X2 - 9.96 X1X3 - 5.51 X1X4 - 4.20 X1X5 - 4.14 X2X3 + 3.84 X2X4
        + 3.99 X2X5 - 1.80 X2X6 - 2.27 X2X7 - 2.74 X2X8 - 3.02 X3X4 + 2.91 X3X5
        + 2.10 X3X7 - 3.43 X4^2 - 7.19 X4X5 - 10.2 X5^2 - 5.82 X7X8 - 15.6 X8^2
        - 1.85 X3X5X6 + 1.82 X5^2X7


Predictor      Coef   SE Coef        T      P
Constant    479.389     1.327   361.27  0.000
X2            4.1955    0.5293     7.93  0.000
X3            7.6276    0.5293    14.41  0.000
X4            7.8747    0.5293    14.88  0.000
X7           15.1964    0.8235    18.45  0.000
X8           30.8168    0.6179    49.88  0.000
X1^2          3.1815    0.5830     5.46  0.000
X1X2         -5.0312    0.6483    -7.76  0.000
X1X3         -9.9569    0.6483   -15.36  0.000
X1X4         -5.5147    0.6483    -8.51  0.000
X1X5         -4.2026    0.6483    -6.48  0.000
X2X3         -4.1426    0.6483    -6.39  0.000
X2X4          3.8398    0.6483     5.92  0.000
X2X5          3.9904    0.6483     6.16  0.000
X2X6         -1.7964    0.5293    -3.39  0.001
X2X7         -2.2660    0.6483    -3.50  0.001
X2X8         -2.7410    0.6482    -4.23  0.000
X3X4         -3.0190    0.6483    -4.66  0.000
X3X5          2.9068    0.6483     4.48  0.000
X3X7          2.0978    0.6483     3.24  0.001
X4^2         -3.4306    0.5301    -6.47  0.000
X4X5         -7.1935    0.6483   -11.10  0.000
X5^2        -10.2248    0.5301   -19.29  0.000
X7X8         -5.8226    0.7574    -7.69  0.000
X8^2        -15.616      1.069   -14.61  0.000
X3X5X6       -1.8497    0.6483    -2.85  0.005
X5^2X7        1.8209    0.6190     2.94  0.003


S = 11.0003   R-Sq = 92.1%   R-Sq(adj) = 91.7%


Analysis of Variance

Source           DF      SS      MS       F      P
Regression       26  634497   24404  201.67  0.000
Residual Error  449   54332     121
Total           475  688829
```
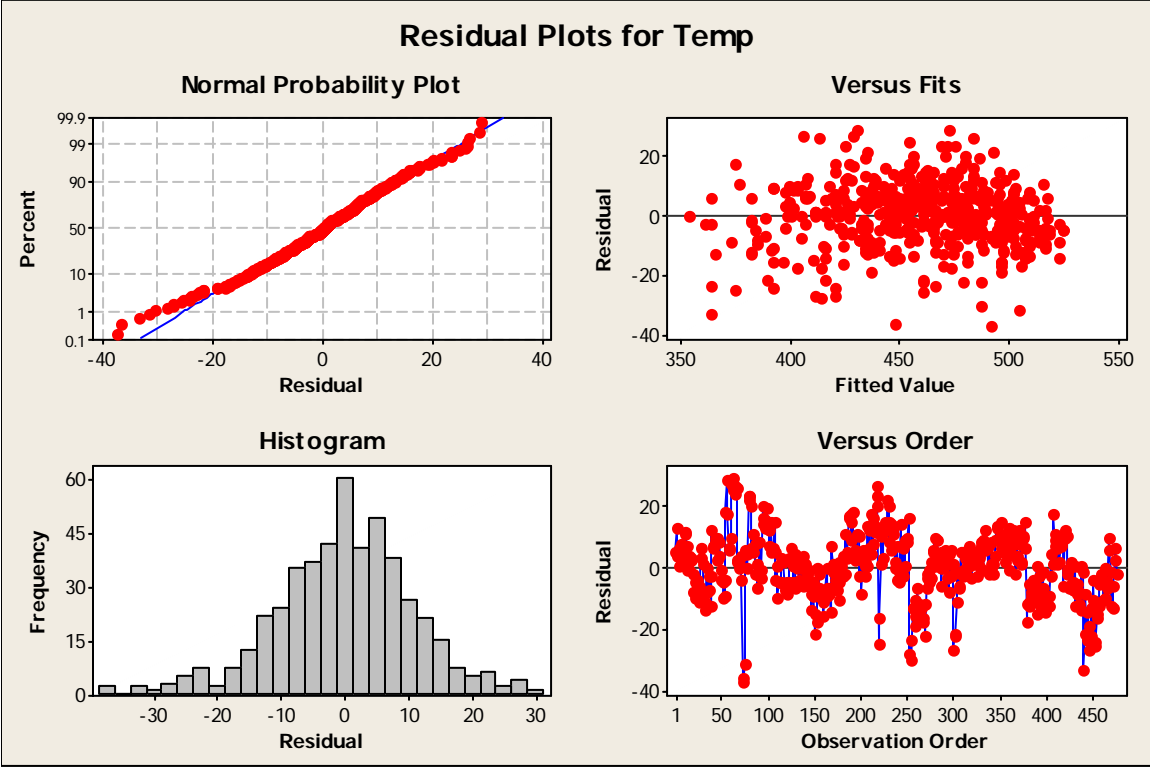
Figure A-4: Residual Plots for Tool Temperature

```
The regression equation is
Torque = 43.6 + 1.70 X2 + 0.734 X5 - 2.75 X6 + 4.94 X7 - 19.1 X8 - 0.588 X1X5
         - 0.466 X2^2 - 0.288 X2X3 - 0.304 X2X7 - 1.64 X2X8 + 0.921 X3X7
         - 0.462 X4^2 + 1.37 X6X8 - 3.29 X7X8 + 10.6 X8^2 + 0.0008 X1^2X6
         + 1.06 X2X8^2 - 0.224 X3^2X6 - 0.417 X3^2X7 - 0.297 X3X5X6
         + 0.732 X3X7^2 - 0.511 X3X7X8 + 0.274 X4X6X7 + 0.339 X5X6X7
         + 1.64 X6X8^2 + 2.13 X7X8^2


Predictor      Coef  SE Coef        T      P
Constant    43.6437   0.1890   230.89  0.000
X2           1.7006   0.1519    11.20  0.000
X5          0.73367  0.08770     8.37  0.000
X6          -2.7457   0.1869   -14.69  0.000
X7           4.9412   0.1956    25.27  0.000
X8         -19.0759   0.1024  -186.34  0.000
X1X5        -0.5878   0.1074    -5.47  0.000
X2^2       -0.46570  0.08603    -5.41  0.000
X2X3        -0.2879   0.1074    -2.68  0.008
X2X7        -0.3038   0.1074    -2.83  0.005
X2X8        -1.6374   0.1074   -15.25  0.000
X3X7         0.9208   0.1074     8.57  0.000
X4^2       -0.46237  0.08603    -5.37  0.000
X6X8         1.3748   0.1024    13.43  0.000
X7X8        -3.2897   0.1255   -26.21  0.000
X8^2        10.6106   0.1771    59.91  0.000
X1^2X6      0.00083  0.09479     0.01  0.993
X2X8^2       1.0565   0.1860     5.68  0.000
X3^2X6     -0.22423  0.08499    -2.64  0.009
X3^2X7      -0.4167   0.1026    -4.06  0.000
X3X5X6      -0.2972   0.1074    -2.77  0.006
X3X7^2       0.7318   0.1074     6.81  0.000
X3X7X8      -0.5107   0.1315    -3.88  0.000
X4X6X7       0.2740   0.1074     2.55  0.011
X5X6X7       0.3393   0.1074     3.16  0.002
X6X8^2       1.6382   0.1771     9.25  0.000
X7X8^2       2.1279   0.2153     9.88  0.000


S = 1.82252   R-Sq = 99.0%   R-Sq(adj) = 99.0%


Analysis of Variance

Source          DF        SS      MS        F      P
Regression      26  149082.6  5733.9  1726.28  0.000
Residual Error 449    1491.4     3.3
Total          475  150574.0
```
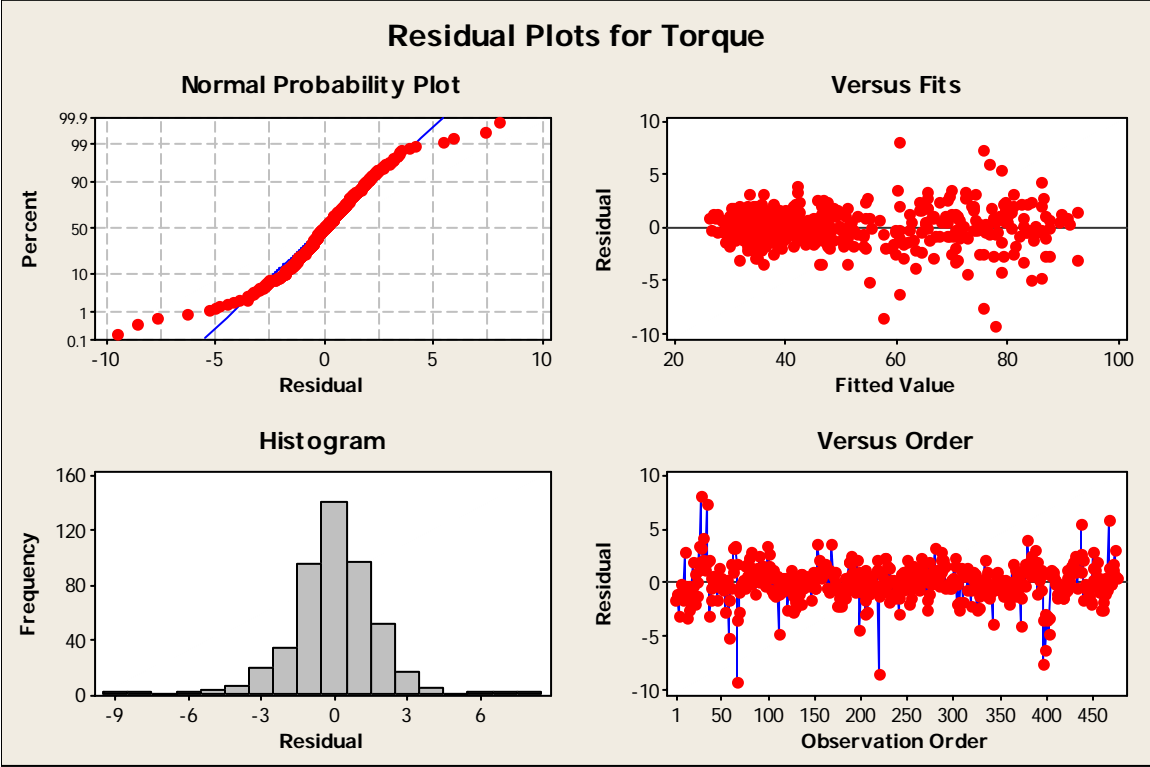
Figure A-5: Residual Plots for Spindle Torque

```
The regression equation is
Discontinuity = 0.158 + 0.237 X1 - 0.0856 X4 + 0.299 X5 + 0.512 X8 + 0.227 X1^2
          + 0.149 X1X5 + 0.140 X1X6 + 0.262 X1X8 - 0.111 X2X7 - 0.194 X2X8
          + 0.219 X3X5 + 0.201 X3X8 - 0.0948 X4^2 - 0.104 X4X8 + 0.134 X5^2
          + 0.271 X5X6 + 0.222 X5X7 + 0.583 X5X8 + 0.246 X6X8 + 0.265 X7X8
          + 0.329 X8^2 + 0.214 X1^2X6 + 0.215 X1^2X7 + 0.205 X1^2X8
          + 0.167 X1X5X8 + 0.104 X1X6X7 + 0.162 X1X6X8 - 0.208 X2X7^2
          + 0.240 X3X5X8 + 0.201 X3X8^2 - 0.121 X4^2X8 + 0.108 X5^2X6
          + 0.0881 X5^2X7 + 0.150 X5^2X8 + 0.278 X5X6X8 + 0.208 X5X7X8
          + 0.285 X5X8^2
```

Predictor	Coef	SE Coef	T	P
Constant	0.15765	0.07367	2.14	0.033
X1	0.23683	0.03151	7.52	0.000
X4	-0.08565	0.02937	-2.92	0.004
X5	0.29861	0.05087	5.87	0.000
X8	0.51159	0.07608	6.72	0.000
X1^2	0.22704	0.03307	6.87	0.000
X1X5	0.14931	0.03597	4.15	0.000
X1X6	0.14031	0.03161	4.44	0.000
X1X8	0.26218	0.03858	6.79	0.000
X2X7	-0.11111	0.03597	-3.09	0.002
X2X8	-0.19444	0.03597	-5.41	0.000
X3X5	0.21875	0.03597	6.08	0.000
X3X8	0.20139	0.03597	5.60	0.000
X4^2	-0.09479	0.02943	-3.22	0.001
X4X8	-0.10417	0.03597	-2.90	0.004
X5^2	0.13438	0.02943	4.57	0.000
X5X6	0.27083	0.02937	9.22	0.000
X5X7	0.22222	0.03597	6.18	0.000
X5X8	0.58333	0.03597	16.22	0.000
X6X8	0.24580	0.03434	7.16	0.000
X7X8	0.26533	0.04206	6.31	0.000
X8^2	0.32882	0.05933	5.54	0.000
X1^2X6	0.21368	0.02566	8.33	0.000
X1^2X7	0.21483	0.03131	6.86	0.000
X1^2X8	0.20482	0.04050	5.06	0.000
X1X5X8	0.16667	0.04405	3.78	0.000
X1X6X7	0.10376	0.03825	2.71	0.007
X1X6X8	0.16224	0.03797	4.27	0.000
X2X7^2	-0.20833	0.03597	-5.79	0.000
X3X5X8	0.23958	0.04405	5.44	0.000
X3X8^2	0.20139	0.03597	5.60	0.000
X4^2X8	-0.12066	0.03604	-3.35	0.001
X5^2X6	0.10817	0.02246	4.82	0.000
X5^2X7	0.08811	0.02749	3.21	0.001
X5^2X8	0.15018	0.03604	4.17	0.000
X5X6X8	0.27778	0.03597	7.72	0.000
X5X7X8	0.20833	0.04405	4.73	0.000
X5X8^2	0.28472	0.06230	4.57	0.000

```
S = 0.610394   R-Sq = 83.1%   R-Sq(adj) = 81.6%
```

Analysis of Variance

Source	DF	SS	MS	F	P
Regression	37	800.558	21.637	58.07	0.000
Residual Error	438	163.190	0.373		
Total	475	963.748			
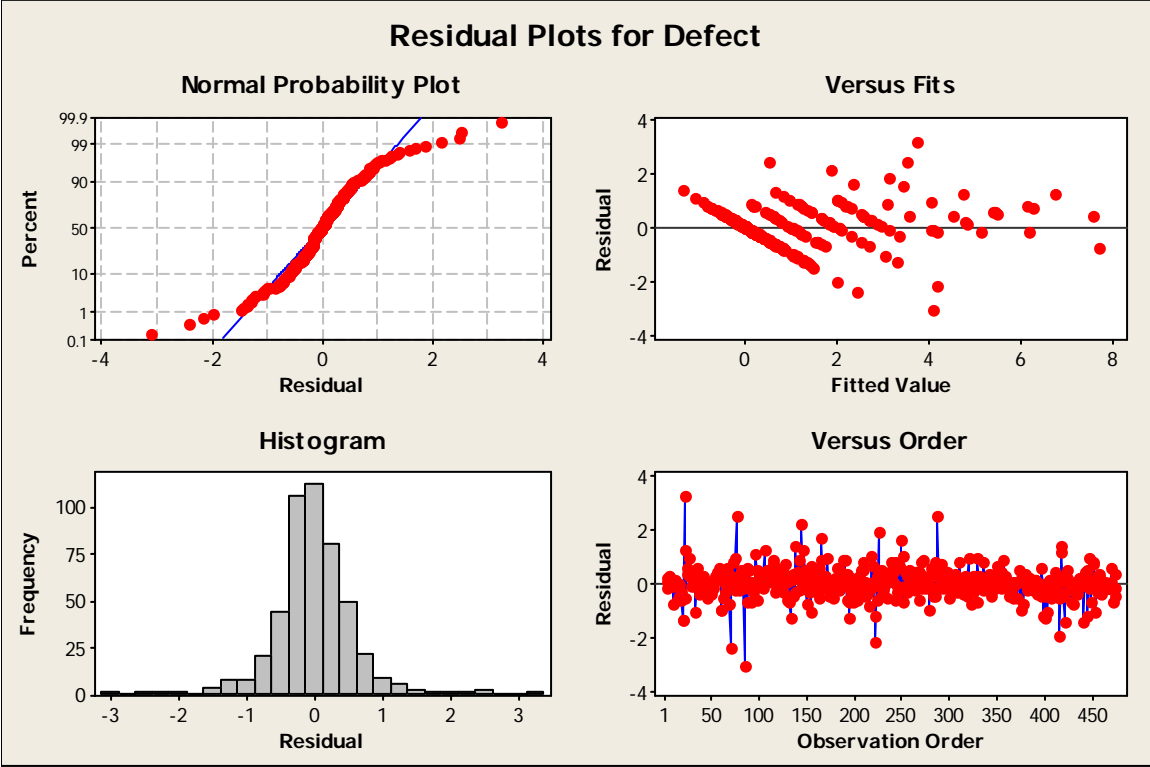
Figure A-6: Residual Plots for Discontinuity Size

```
The regression equation is
Flash = 3.54 + 0.732 X2 + 0.854 X3 + 0.498 X5 + 0.588 X6 + 1.38 X7 + 1.53 X8
        + 0.151 X1^2 + 0.150 X2X4 + 0.175 X2X7 + 0.230 X3X5 + 0.179 X3X6
        + 0.230 X3X7 - 0.154 X4^2 + 0.185 X4X7 - 0.272 X5^2 + 0.257 X5X6
        + 0.199 X5X7 + 0.380 X5X8 + 0.193 X6X7 + 0.223 X7X8 + 0.179 X1X5X7
        + 0.200 X2X4X7 - 0.164 X3^2X7 + 0.231 X4X5X7 + 0.151 X4X6X7
        + 0.151 X5X6X7 - 0.246 X6X7X8


Predictor      Coef   SE Coef      T       P
Constant    3.54234   0.08660   40.90   0.000
X2          0.73179   0.04097   17.86   0.000
X3          0.85448   0.04097   20.86   0.000
X5          0.49799   0.04097   12.15   0.000
X6          0.58827   0.03905   15.06   0.000
X7          1.37791   0.06378   21.60   0.000
X8          1.52596   0.04783   31.90   0.000
X1^2        0.15121   0.04517    3.35   0.001
X2X4        0.14977   0.05018    2.98   0.003
X2X7        0.17488   0.05018    3.49   0.001
X3X5        0.22963   0.05018    4.58   0.000
X3X6        0.17855   0.04097    4.36   0.000
X3X7        0.23044   0.05018    4.59   0.000
X4^2       -0.15426   0.04104   -3.76   0.000
X4X7        0.18530   0.05018    3.69   0.000
X5^2       -0.27232   0.04104   -6.64   0.000
X5X6        0.25725   0.04097    6.28   0.000
X5X7        0.19919   0.05018    3.97   0.000
X5X8        0.38021   0.05018    7.58   0.000
X6X7        0.19343   0.04789    4.04   0.000
X7X8        0.22282   0.05863    3.80   0.000
X1X5X7      0.17899   0.06146    2.91   0.004
X2X4X7      0.19982   0.06146    3.25   0.001
X3^2X7     -0.16401   0.04793   -3.42   0.001
X4X5X7      0.23107   0.06146    3.76   0.000
X4X6X7      0.15058   0.05018    3.00   0.003
X5X6X7      0.15058   0.05018    3.00   0.003
X6X7X8     -0.24592   0.05863   -4.19   0.000


S = 0.851524   R-Sq = 87.7%   R-Sq(adj) = 86.9%


Analysis of Variance

Source          DF       SS      MS       F      P
Regression      27  2306.366  85.421  117.81  0.000
Residual Error 448   324.841   0.725
Total          475  2631.207
```
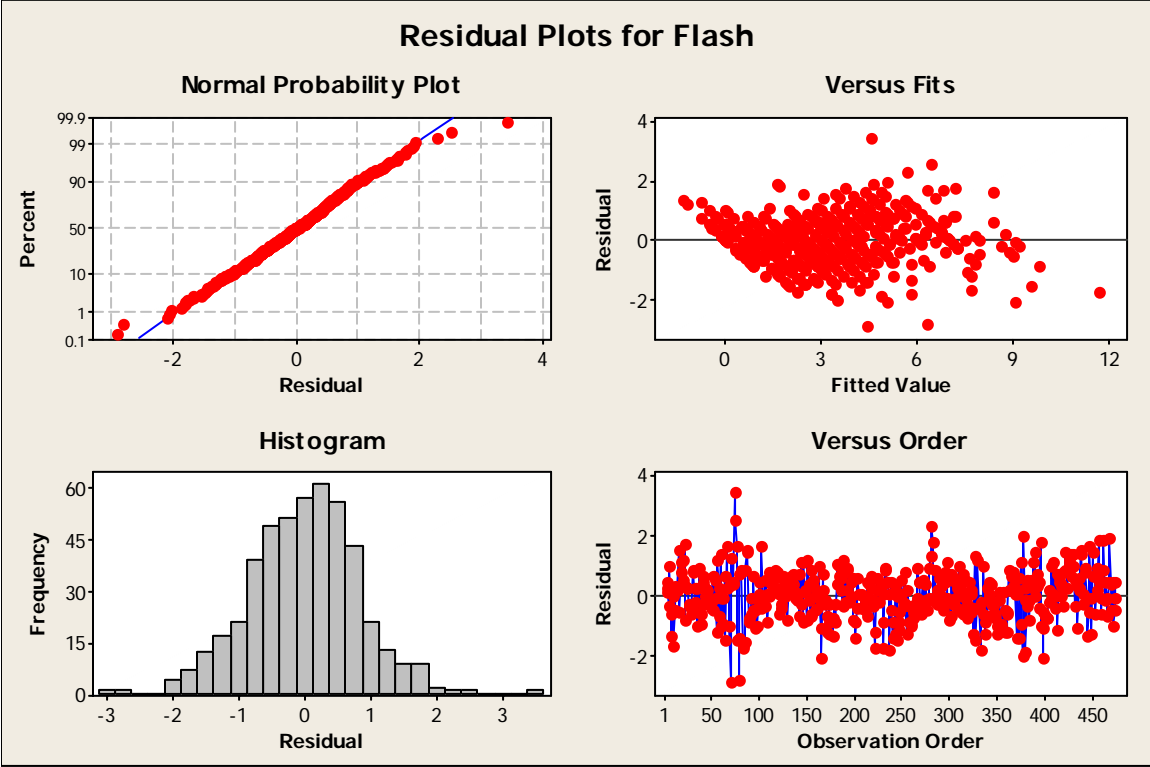
Figure A-7: Residual Plots for Amount of Flash

```
The regression equation is
Rough = 5.70 + 0.384 X2 + 0.310 X3 + 0.310 X5 + 0.330 X6 + 0.972 X7 + 2.17 X8
        + 0.123 X1^2 + 0.173 X1X5 + 0.132 X2X4 - 0.187 X2X7 + 0.156 X2X8
        + 0.180 X3X5 - 0.184 X4X8 - 0.318 X5^2 + 0.323 X5X8 + 0.376 X7X8
        - 0.312 X8^2 - 0.197 X3X5X7 - 0.134 X5^2X8 - 0.354 X7X8^2


Predictor      Coef   SE Coef       T      P
Constant    5.69708   0.08582   66.38  0.000
X2          0.38407   0.04028    9.54  0.000
X3          0.30999   0.04028    7.70  0.000
X5          0.30999   0.04028    7.70  0.000
X6          0.33032   0.03838    8.61  0.000
X7          0.97225   0.07957   12.22  0.000
X8          2.17365   0.06365   34.15  0.000
X1^2        0.12322   0.04345    2.84  0.005
X1X5        0.17332   0.04933    3.51  0.000
X2X4        0.13166   0.04933    2.67  0.008
X2X7       -0.18721   0.04933   -3.79  0.000
X2X8        0.15625   0.04933    3.17  0.002
X3X5        0.18027   0.04933    3.65  0.000
X4X8       -0.18403   0.04933   -3.73  0.000
X5^2       -0.31805   0.03903   -8.15  0.000
X5X8        0.32292   0.04933    6.55  0.000
X7X8        0.37602   0.05763    6.52  0.000
X8^2       -0.31222   0.08135   -3.84  0.000
X3X5X7     -0.19748   0.06042   -3.27  0.001
X5^2X8     -0.13370   0.04722   -2.83  0.005
X7X8^2     -0.35389   0.09885   -3.58  0.000


S = 0.837090   R-Sq = 85.6%   R-Sq(adj) = 84.9%


Analysis of Variance

Source           DF        SS       MS       F      P
Regression       20  1890.742   94.537  134.91  0.000
Residual Error  455   318.827    0.701
Total           475  2209.569
```
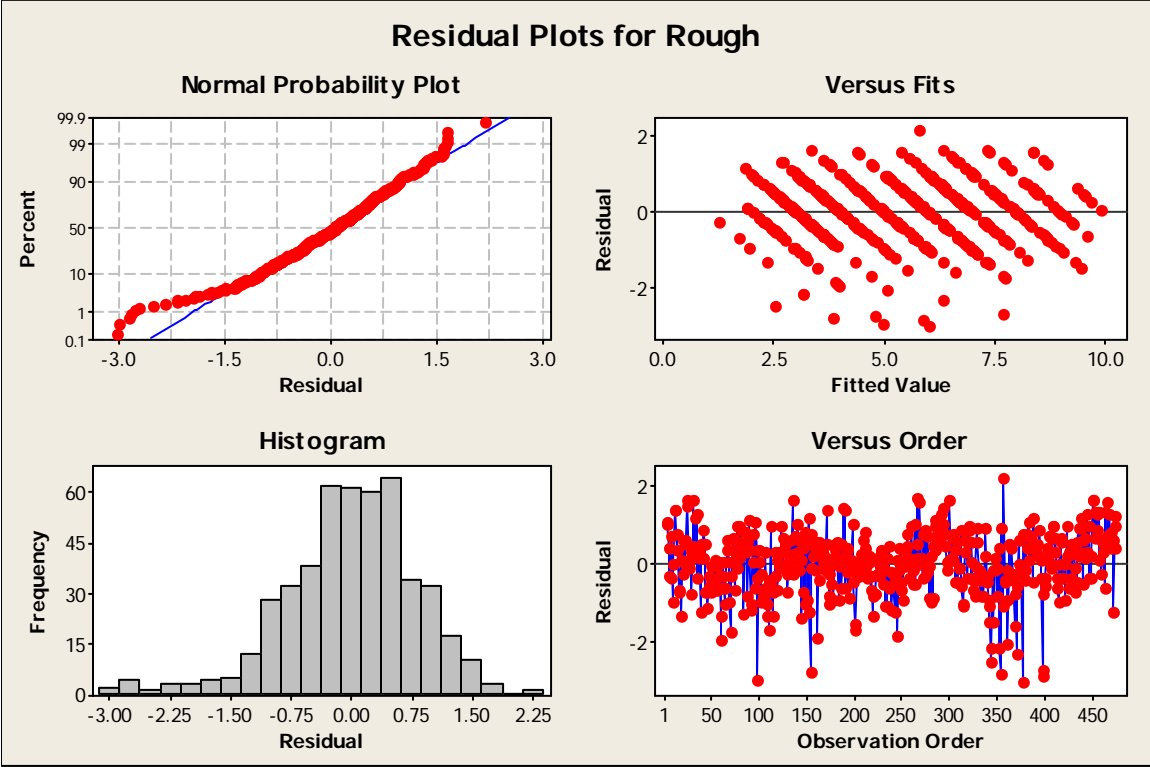
Figure A-8: Residual Plots for Surface Roughness

```
The regression equation is
Ledge = 4.73 + 0.307 X2 + 0.522 X3 + 0.312 X5 + 0.999 X6 + 1.06 X7 + 3.01 X8
        + 0.381 X1X5 - 0.178 X3^2 + 0.371 X3X7 - 0.251 X4^2 + 0.214 X4X5
        - 0.331 X5^2 + 0.166 X5X6 + 0.342 X5X8 + 0.399 X6X8 + 0.506 X7X8
        + 0.247 X1X5X8 - 0.199 X2X6X7 - 0.252 X3^2X8 + 0.218 X4X6X7
        - 0.262 X5^2X8 - 0.366 X6X8^2


Predictor      Coef   SE Coef      T       P
Constant     4.7314    0.1335   35.45   0.000
X2           0.30711  0.05995    5.12   0.000
X3           0.52238  0.05995    8.71   0.000
X5           0.31174  0.05995    5.20   0.000
X6           0.99938  0.09883   10.11   0.000
X7           1.05664  0.06906   15.30   0.000
X8            3.0093   0.1240   24.27   0.000
X1X5         0.38080  0.07343    5.19   0.000
X3^2        -0.17797  0.06131   -2.90   0.004
X3X7         0.37094  0.07343    5.05   0.000
X4^2        -0.25088  0.06131   -4.09   0.000
X4X5         0.21413  0.07343    2.92   0.004
X5^2        -0.33075  0.06131   -5.39   0.000
X5X6         0.16590  0.05995    2.77   0.006
X5X8         0.34201  0.07342    4.66   0.000
X6X8         0.39866  0.06999    5.70   0.000
X7X8         0.50644  0.08579    5.90   0.000
X1X5X8       0.24740  0.08993    2.75   0.006
X2X6X7      -0.19851  0.07343   -2.70   0.007
X3^2X8      -0.25152  0.07207   -3.49   0.001
X4X6X7       0.21816  0.07343    2.97   0.003
X5^2X8      -0.26193  0.07207   -3.63   0.000
X6X8^2       -0.3656   0.1211   -3.02   0.003


S = 1.24604   R-Sq = 82.1%   R-Sq(adj) = 81.3%


Analysis of Variance

Source          DF       SS      MS      F       P
Regression      22  3231.91  146.91  94.62   0.000
Residual Error 453   703.33    1.55
Total          475  3935.25
```
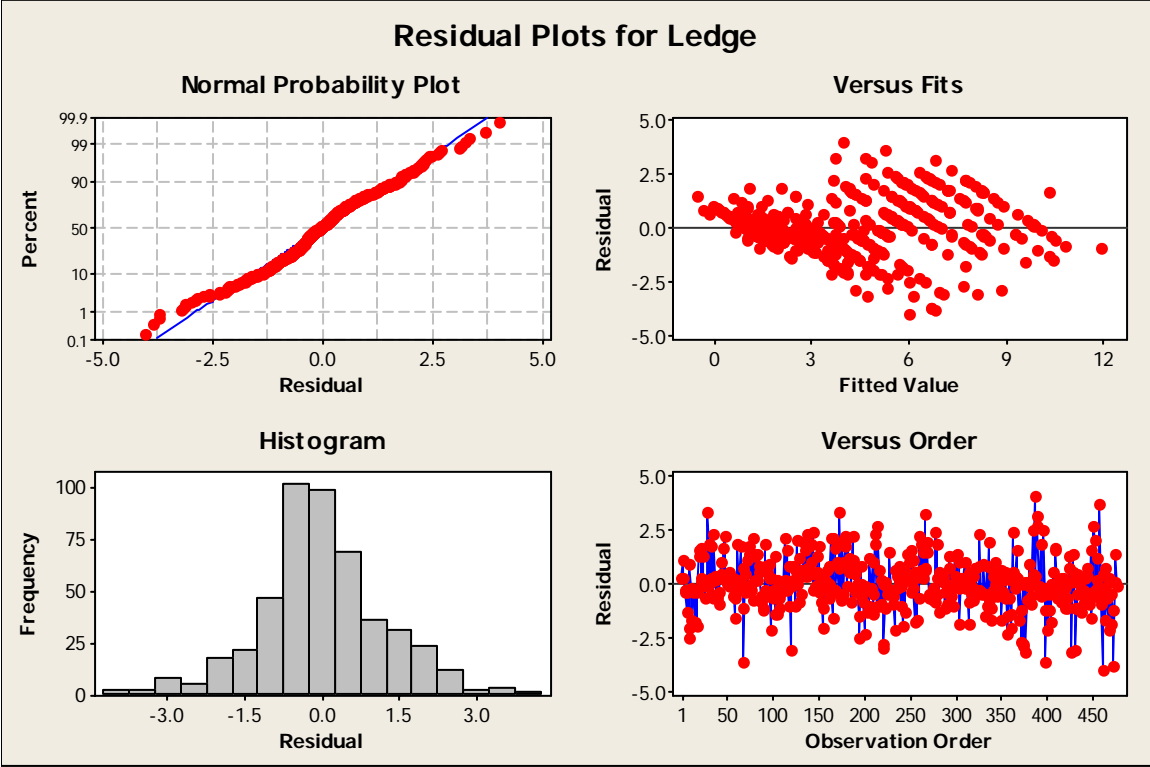
Figure A-9: Residual Plots for Ledge Size

Appendix B.   Optimization Tables for Response Surfaces

Table B-1: Minimum Lateral Forces (Y)

X1	X2	X3	X4	X5	X6	X7	X8	Minimum	#
0.45	0.10	0.30	0.11	-2.16	-1.00	-1.00	0.17	830	3
0.28	0.29	-0.25	0.19	2.18	-1.00	-1.00	-1.00	760	4
0.53	0.35	0.78	0.45	-1.95	1.00	1.00	1.00	90	9
0.81	-0.35	0.05	-1.00	-1.00	-1.00	-1.00	-0.23	1640	3
0.55	0.13	-0.33	1.00	1.00	-1.00	-1.00	-1.00	1510	4
1.00	1.00	1.00	1.00	-1.00	1.00	1.00	1.00	980	4
0.55	0.13	-0.33	-1.00	1.00	-1.00	-1.00	-1.00	1580	1
1.00	1.00	-0.52	1.00	-1.00	-1.00	-1.00	0.71	1610	3
1.00	-0.13	-1.00	1.00	1.00	-1.00	-1.00	1.00	1780	1

Table B-2: Maximum Lateral Forces (Y)

X1	X2	X3	X4	X5	X6	X7	X8	Maximum	#
-1.94	0.12	1.04	-0.04	0.40	1.00	1.00	-1.00	7290	16
-1.00	1.00	1.00	-0.13	0.85	1.00	1.00	-1.00	6430	6
-1.00	-1.00	1.00	-1.00	1.00	-1.00	1.00	1.00	5750	5
1.00	1.00	1.00	-0.13	0.85	1.00	1.00	-1.00	5620	2
-1.00	-1.00	1.00	-0.13	1.00	1.00	1.00	-1.00	6460	3

Table B-3: Minimum Axial Forces (Z)

X1	X2	X3	X4	X5	X6	X7	X8	Minimum	#
-0.62	-2.04	-0.58	0.05	0.34	-1.00	-1.00	-1.00	13130	7
-0.54	-1.95	-0.86	0.06	0.43	-1.00	-1.00	-0.20	13080	2
-1.40	-1.68	-0.28	-0.06	-0.37	-1.00	-1.00	1.00	12340	7
-1.00	-1.00	-0.29	-1.00	-1.00	-1.00	-1.00	-1.00	16660	4
-1.00	-1.00	-1.00	1.00	1.00	-1.00	-1.00	-0.01	15420	3
-1.00	-1.00	-0.81	-1.00	-0.61	-1.00	-1.00	1.00	15040	8
1.00	-1.00	-1.00	1.00	1.00	-1.00	-1.00	-0.01	16190	1

Table B-4: Maximum Axial Forces (Z)

X1	X2	X3	X4	X5	X6	X7	X8	Maximum	#
0.22	0.22	0.24	-0.46	2.15	1.00	1.00	1.00	43970	4
0.95	0.51	0.71	0.33	-1.79	1.00	1.00	0.10	48800	12
1.00	0.87	1.00	1.00	-1.00	1.00	1.00	-0.15	47260	16

Table B-5: Minimum Tool Temperature

X1	X2	X3	X4	X5	X6	X7	X8	Minimum	#
-0.50	0.00	-0.41	-1.11	-1.83	1.00	-1.00	-1.00	333	8
0.01	-0.80	-0.60	0.35	1.97	-1.00	-1.00	-1.00	336	8
-1.00	-1.00	-1.00	-1.00	-1.00	1.00	-1.00	-1.00	349	7
-1.00	-1.00	-1.00	-1.00	1.00	-1.00	-1.00	-1.00	354	4
-0.83	-1.00	-1.00	1.00	1.00	-1.00	-1.00	-1.00	365	3
0.83	1.00	1.00	-1.00	-1.00	-1.00	-1.00	-1.00	382	1
1.00	-1.00	1.00	1.00	1.00	1.00	-1.00	-1.00	378	1

Table B-6: Maximum Tool Temperature

X1	X2	X3	X4	X5	X6	X7	X8	Maximum	#
-1.64	0.41	1.34	0.48	0.33	-1.00	1.00	0.76	559	10
1.92	-0.98	-0.43	-0.12	-0.40	1.00	1.00	0.89	534	6
-1.00	1.00	1.00	1.00	0.34	-1.00	1.00	0.71	542	10
1.00	-1.00	1.00	-0.38	-0.26	1.00	1.00	0.89	521	3
1.00	1.00	-1.00	1.00	-0.72	-1.00	1.00	0.71	519	3

Table B-7: Minimum Spindle Torque

X1	X2	X3	X4	X5	X6	X7	X8	Minimum	#
-0.29	-2.10	-0.45	0.38	-0.42	1.00	-1.00	0.71	34.0	11
-0.31	-0.96	-1.82	-0.20	-0.79	1.00	1.00	0.69	41.4	3
-0.16	-2.08	-0.25	-0.38	-0.66	-1.00	-1.00	1.00	34.0	2
-1.00	-1.00	-1.00	-1.00	-1.00	1.00	-1.00	0.73	36.4	3
-0.75	-1.00	-0.24	-1.00	-1.00	-1.00	-1.00	1.00	36.9	2
1.00	-1.00	-1.00	-1.00	-1.00	1.00	-1.00	0.73	38.0	3
-1.00	-1.00	-1.00	1.00	-1.00	1.00	-1.00	0.73	35.7	4
1.00	-1.00	-0.44	1.00	1.00	1.00	-1.00	0.72	37.5	2
1.00	-1.00	-1.00	1.00	-1.00	1.00	-1.00	0.73	37.3	2

Table B-8: Maximum Spindle Torque

X1	X2	X3	X4	X5	X6	X7	X8	Maximum	#
-0.75	1.61	1.08	-0.12	0.82	-1.00	1.00	-1.00	127.9	16
-1.00	1.00	1.00	-0.30	1.00	-1.00	1.00	-1.00	126.4	7
1.00	1.00	1.00	-0.30	1.00	-1.00	1.00	-1.00	124.8	6
-0.75	0.72	0.50	0.30	1.00	1.00	1.00	1.00	55.7	3

Table B-9: Minimum Discontinuity Size

X1	X2	X3	X4	X5	X6	X7	X8	Minimum	#
-0.09	-0.15	-0.07	0.31	-2.21	-1.00	-1.00	-1.00	-1.3	2
-0.17	0.51	0.00	2.17	-0.01	1.00	1.00	-1.00	-1.6	7
-0.43	0.09	-0.51	0.16	2.13	-1.00	-1.00	-0.23	-1.6	3
-0.58	1.11	0.43	1.23	-1.31	1.00	1.00	1.00	-1.5	2
-0.49	0.68	0.58	1.38	-1.43	1.00	-1.00	1.00	-1.2	2
-0.15	-1.00	-1.00	-1.00	-0.04	1.00	0.40	-1.00	-0.7	4
-1.00	1.00	-1.00	1.00	1.00	-1.00	-1.00	1.00	-1.2	2
-0.28	1.00	-1.00	-1.00	-0.05	1.00	1.00	-1.00	-0.8	1
-0.71	1.00	1.00	-1.00	-0.49	1.00	1.00	-0.46	-0.9	1
-1.00	1.00	-1.00	-1.00	1.00	-1.00	-1.00	0.29	-0.8	1
-1.00	1.00	1.00	1.00	-1.00	1.00	1.00	1.00	-1.2	1
-0.15	-1.00	-0.79	1.00	-0.03	1.00	0.40	-1.00	-0.9	1
-0.28	1.00	-0.84	1.00	-0.04	1.00	1.00	-1.00	-1.1	1
-1.00	1.00	1.00	1.00	-1.00	1.00	-1.00	1.00	-0.9	2
-0.15	-1.00	-0.19	1.00	-0.01	1.00	0.40	-1.00	-0.9	1
-0.28	1.00	-0.03	1.00	-0.02	1.00	1.00	-1.00	-1.1	1

Table B-10: Maximum Discontinuity Size

X1	X2	X3	X4	X5	X6	X7	X8	Maximum	#
0.86	-0.20	0.52	-0.13	1.98	1.00	1.00	1.00	10.8	16
1.00	-1.00	1.00	-1.00	1.00	1.00	1.00	1.00	7.8	11
-1.00	-1.00	-1.00	-1.00	-1.00	-1.00	-1.00	1.00	1.3	1
1.00	1.00	1.00	-0.76	-0.07	-1.00	-0.97	-1.00	0.5	1
-1.00	-1.00	-1.00	-1.00	-1.00	-1.00	1.00	1.00	1.8	1
-1.00	1.00	-1.00	-0.75	0.08	-1.00	-0.46	-1.00	0.5	1
-1.00	1.00	1.00	-0.76	-0.01	-1.00	-0.47	-1.00	0.5	1

Table B-11: Minimum Flash

X1	X2	X3	X4	X5	X6	X7	X8	Minimum	#
-0.30	-0.99	-0.09	-1.20	-1.57	-1.00	-1.00	-1.00	-1.0	4
-0.15	-0.92	-1.71	0.05	1.09	-1.00	1.00	-1.00	-1.6	3
0.28	-0.60	-0.73	0.78	1.85	-1.00	-1.00	-1.00	-2.0	6
-0.37	-0.96	-0.40	-0.49	-1.88	1.00	-1.00	-1.00	-0.9	2
0.23	-0.57	-0.96	1.17	1.53	1.00	-1.00	-1.00	-1.9	1
-0.59	-1.00	-0.66	-1.00	-1.00	-1.00	-1.00	-1.00	-0.5	4
0.59	-1.00	-1.00	-1.00	1.00	-1.00	-1.00	-1.00	-0.8	3
0.59	-1.00	-1.00	1.00	1.00	1.00	-1.00	-1.00	-1.4	4
-0.59	-1.00	-1.00	1.00	-1.00	1.00	-1.00	-1.00	-0.5	3
-0.59	-1.00	-1.00	1.00	-1.00	1.00	-1.00	-1.00	-0.5	2

Table B-12: Maximum Fash

X1	X2	X3	X4	X5	X6	X7	X8	Maximum	#
0.32	1.16	1.16	0.78	1.27	1.00	1.00	1.00	12.1	16
1.00	1.00	1.00	1.00	1.00	1.00	1.00	1.00	11.7	10
-1.00	1.00	1.00	1.00	1.00	1.00	1.00	1.00	11.4	6

Table B-13: Minimum Surface Roughness

X1	X2	X3	X4	X5	X6	X7	X8	Minimum	#
-0.30	-0.56	-1.33	-0.16	1.67	-1.00	-1.00	-1.00	0.5	9
0.51	0.05	-0.83	-0.46	-1.96	-1.00	1.00	-1.00	1.9	1
0.42	-0.72	0.76	-0.16	-1.93	-1.00	-1.00	-1.00	1.2	6
-0.70	-1.00	-1.00	-1.00	1.00	-1.00	-1.00	-1.00	1.2	9
0.70	1.00	-1.00	-1.00	-1.00	-1.00	1.00	-1.00	2.3	1
0.70	-1.00	1.00	-1.00	-1.00	-1.00	-1.00	-1.00	1.9	6

Table B-14: Maximum Surface Roughness

X1	X2	X3	X4	X5	X6	X7	X8	Maximum	#
1.60	1.02	0.91	-0.15	0.73	1.00	1.00	1.00	10.3	16
-1.00	1.00	1.00	-1.00	0.49	1.00	1.00	1.00	9.8	8
1.00	1.00	1.00	-1.00	0.87	1.00	1.00	1.00	10.1	8

Table B-15: Minimum Ledge Size

X1	X2	X3	X4	X5	X6	X7	X8	Minimum	#
-0.08	-0.17	-0.19	-2.19	0.37	-1.00	-1.00	-1.00	-1.0	6
0.02	-0.79	-1.14	1.75	-0.10	-1.00	1.00	-1.00	-0.4	4
0.07	-0.79	-0.19	2.06	-0.32	1.00	-1.00	-1.00	-0.7	5
-0.03	-0.17	-1.14	-1.91	0.15	1.00	1.00	-1.00	0.2	1
-1.00	-1.00	-1.00	-1.00	0.46	-1.00	-1.00	-1.00	0.2	8
1.00	-1.00	-1.00	1.00	-0.41	1.00	-1.00	-1.00	0.2	5
-1.00	-1.00	-1.00	1.00	0.10	-1.00	1.00	-1.00	0.2	3

Table B-16: Maximum Ledge Size

X1	X2	X3	X4	X5	X6	X7	X8	Maximum	#
-1.77	0.27	0.71	-0.03	-1.13	1.00	1.00	1.00	11.2	6
1.12	0.11	0.47	0.40	1.83	1.00	1.00	1.00	13.9	10
1.00	1.00	1.00	0.86	1.00	1.00	1.00	1.00	12.6	16